

## FORMATION OF $Z \sim 6$ QUASARS FROM HIERARCHICAL GALAXY MERGERS

YUEXING LI<sup>1</sup>, LARS HERNQUIST<sup>1</sup>, BRANT ROBERTSON<sup>1,2,7</sup>, THOMAS J. COX<sup>1</sup>, PHILIP F. HOPKINS<sup>1</sup>, VOLKER SPRINGEL<sup>3</sup>, LIANG GAO<sup>4</sup>, TIZIANA DI MATTEO<sup>5</sup>, ANDREW R. ZENTNER<sup>2</sup>, ADRIAN JENKINS<sup>4</sup>, NAOKI YOSHIDA<sup>6</sup>

<sup>1</sup>Harvard-Smithsonian Center for Astrophysics, Harvard University, 60 Garden Street, Cambridge, MA 02138, USA

<sup>2</sup>Kavli Inst. for Cosmological Physics, Dept. of Astronomy & Astrophysics, Univ. of Chicago, 933 East 56th Street, Chicago, IL 60637, USA

<sup>3</sup>Max-Planck-Institute for Astrophysics, Karl-Schwarzschild-Str. 1, 85740 Garching, Germany

<sup>4</sup>Inst. for Computational Cosmology, Dep. of Physics, Univ. of Durham, South Road, Durham DH1 3LE, UK

<sup>5</sup>Dept. of Physics, Carnegie-Mellon University, 5000 Forbes Ave., Pittsburgh, PA 15213, USA

<sup>6</sup>Nagoya University, Dept. of Physics, Nagoya, Aichi 464-8602, Japan and

<sup>7</sup>Spitzer Fellow

Accepted to ApJ

### ABSTRACT

The discovery of luminous quasars at redshift  $z \sim 6$  indicates the presence of supermassive black holes (SMBHs) of mass  $\sim 10^9 M_\odot$  when the Universe was less than one billion years old. This finding presents several challenges for theoretical models, because whether such massive objects can form so early in the  $\Lambda$ -cold dark matter ( $\Lambda$ CDM) cosmology, the leading theory for cosmic structure formation, is an open question. Furthermore, whether the formation process requires exotic physics such as super-Eddington accretion remains undecided. Here, we present the first multi-scale simulations that, together with a self-regulated model for the SMBH growth, produce a luminous quasar at  $z \sim 6.5$  in the  $\Lambda$ CDM paradigm. We follow the hierarchical assembly history of the most massive halo in a  $\sim 3 \text{ Gpc}^3$  volume, and find that this halo of  $\sim 8 \times 10^{12} M_\odot$  forming at  $z \sim 6.5$  after several major mergers is able to reproduce a number of observed properties of SDSS J1148+5251, the most distant quasar detected at  $z = 6.42$  (Fan et al. 2003). Moreover, the SMBHs grow through gas accretion below the Eddington limit in a self-regulated manner owing to feedback. We find that the progenitors experience vigorous star formation (up to  $10^4 M_\odot \text{ yr}^{-1}$ ) preceding the major quasar phase such that the stellar mass of the quasar host reaches  $10^{12} M_\odot$  at  $z \sim 6.5$ , consistent with observations of significant metal enrichment in SDSS J1148+5251. The merger remnant thus obeys similar  $M_{\text{BH}}-M_{\text{bulge}}$  scaling relation observed locally as a consequence of coeval growth and evolution of the SMBH and its host galaxy. Our results provide a viable formation mechanism for  $z \sim 6$  quasars in the standard  $\Lambda$ CDM cosmology, and demonstrate a common, merger-driven origin for the rarest quasars and the fundamental  $M_{\text{BH}}-M_{\text{bulge}}$  correlation in a hierarchical Universe.

*Subject headings:* black hole physics — cosmology: theory, early Universe — galaxies: active, formation, evolution, starburst, high-redshift, ISM — methods: numerical — quasars: general, individual (SDSS J1148+5251)

### 1. INTRODUCTION

Quasars rank among the most luminous objects in the Universe and are believed to be powered by SMBHs (e.g., Salpeter 1964; Lynden-Bell 1969). They constrain the formation and evolution of galaxies and SMBHs throughout cosmic time. The similarity between the cosmic star formation history (e.g., Madau et al. 1996; Bunker et al. 2004; Bouwens et al. 2004) and the evolution of quasar abundances (e.g., Shaver et al. 1996) suggests an intriguing link between galaxy formation and black hole growth. This is strengthened by tight correlations measured locally between the masses of the black holes and the global properties of the spheroid components of their hosts, such as their luminosities and masses (Magorrian et al. 1998; Marconi & Hunt 2003), light concentration (Graham et al. 2001), and velocity dispersions (Ferrarese & Merritt 2000; Gebhardt et al. 2000; Tremaine et al. 2002).

Distant, highly luminous quasars are important cosmological probes for studying the first generation of galaxies, the star formation history and metal enrichment in the early Universe, the growth of the first supermassive black holes (SMBHs), the role of feedback from quasars and black holes in galaxy evo-

lution, and the epoch of reionization. The Sloan Digital Sky Survey (SDSS, York et al. 2000) has contributed significantly to the discovery of high redshift quasars. Currently, there are over 1000 quasars known at  $z \gtrsim 4$  and 12 at  $z \gtrsim 6$  (Fan et al. 2001, 2003, 2004, 2006). As reviewed by Fan (2006), quasars at  $z \sim 6$  are characterized by: (1) a low space density ( $\sim 10^{-9} \text{ Mpc}^{-3}$  comoving); (2) high luminosities (absolute luminosity at rest-frame  $M_{1450} < -26$ ), believed to be powered by SMBHs of  $\sim 10^9 M_\odot$ ; (3) Gunn-Peterson absorption troughs (Gunn & Peterson 1965) in their spectra, which place these quasars at the end of the epoch of reionization (e.g., Fan et al. 2001; Becker et al. 2001; Djorgovski et al. 2001; Lidz et al. 2002; Songaila & Cowie 2002; White et al. 2003; Sokasian et al. 2003); and (4) a lack of evolution in the spectral energy distribution compared to lower-shift counterparts (e.g., Elvis et al. 1994; Glikman et al. 2006; Richards et al. 2006), which demonstrates the existence of “mature” quasars at early times and comparable metal enrichment in quasars at all cosmic epochs.

The most distant quasar known, SDSS J1148+5251 (hereafter J1148+5251), was discovered by SDSS at  $z = 6.42$  (Fan et al. 2003). It is extremely bright optically with  $M_{1450} = -27.8$ , and deep imaging surveys in both optical and radio (Carilli et al. 2004; White et al. 2005; Willott et al. 2005)

show no sign of gravitational lensing or other companions at the same redshift in the vicinity. Over the past few years, this quasar has been extensively studied at many wavelengths. Near-infrared observations by Willott et al. (2003) and Barth et al. (2003) imply a bolometric luminosity of  $L_{\text{bol}} \sim 10^{14} L_{\odot}$  powered by accretion onto a SMBH of mass  $1-5 \times 10^9 M_{\odot}$ . Radio observations by Bertoldi et al. (2003a) and Carilli et al. (2004) suggest that the host is a hyper-luminous far-infrared (FIR) galaxy, with  $L_{\text{FIR}} \sim 10^{13} L_{\odot}$ , and these authors estimate a star formation rate of  $\sim 3 \times 10^3 M_{\odot} \text{yr}^{-1}$  by assuming most of the FIR luminosity comes from young stars. Emission from carbon monoxide (CO) has been detected (Walter et al. 2003; Bertoldi et al. 2003b; Walter et al. 2004) corresponding to a mass of  $\sim 2 \times 10^{10} M_{\odot}$ . Dust has been seen by several groups (e.g., Robson et al. 2004; Bertoldi et al. 2003a; Carilli et al. 2004; Beelen et al. 2006) with an estimated mass of  $\sim 5 \times 10^8 M_{\odot}$ . In particular, *Spitzer* observations by Charmandaris et al. (2004) and Hines et al. (2006) indicate that the dust is heated by an active galactic nucleus (AGN). Furthermore, the detection of iron by Barth et al. (2003), the carbon fine structure line [CII] by Maiolino et al. (2005) and excess OI absorption by Becker et al. (2006) indicate near-solar metallicity in the quasar host.

These observations raise many fundamental questions for models of quasar and galaxy formation: Where do such high-redshift, luminous quasars originate? How do they form? What are the mechanisms and physical conditions for SMBH growth? And, do these quasar hosts obey the same SMBH–host correlations as observed in the local Universe?

Interpretations of various observations of J1148+5251 have painted a rather conflicting picture for the formation site of the quasar halo and the SMBH–host relationship. The low abundance of these quasars leads to the view that they are hosted by massive halos ( $\gtrsim 10^{13} M_{\odot}$ ) in the rarest density peaks of the dark matter distribution (Fan et al. 2003). However, it has been argued, based on the lack of companion galaxies in the field, that this quasar may reside in a much lower mass halo in a less overdense region (Carilli et al. 2004; Willott et al. 2005). Moreover, Walter et al. (2004) suggest, based on the dynamical mass estimate from CO measurements, that J1148+5251 contains a small stellar spheroid, and that the SMBH may have largely formed before the host galaxy. However, the detection of metal lines (Walter et al. 2004; Barth et al. 2003; Maiolino et al. 2005), along with dust (Bertoldi et al. 2003a; Carilli et al. 2004; Robson et al. 2004; Charmandaris et al. 2004; Hines et al. 2006; Beelen et al. 2006), indicates that the interstellar medium (ISM) of J1148+5251 was significantly enriched by heavy elements produced through massive star formation at rates of  $\sim 10^3 M_{\odot} \text{yr}^{-1}$  occurring as early as  $z \gtrsim 10$ , and that large stellar bulges form before accreting SMBHs undergo luminous quasar activity.

In an expanding Universe that is dominated by cold dark matter and is accelerated by dark energy, the  $\Lambda$ -cold dark matter ( $\Lambda$ CDM) cosmology, the leading theoretical model for structure formation, assumes that structure grows from weak density fluctuations amplified by gravity, with small objects collapsing first and subsequently merging to form progressively more massive ones, a process known as “hierarchical assembly” (e.g., see Barkana & Loeb 2001 for a review). The formation of galaxies and quasars is therefore determined by the abundance of dark matter halos; i.e., the number density of halos as a function of mass and redshift. The most

widely used analytic model for the halo mass function was first developed by Press & Schechter (1974) (hereafter PS), which is based on Gaussian density perturbations, linear gravitational growth, and spherical collapse of dark matter. Using the PS mass functions, Efstathiou & Rees (1988) studied the abundance of rare objects, such as luminous quasars at high redshifts. These authors predicted a sharp “cut-off” of the quasar population at  $z \sim 5$ . However, while the initial, linear growth of density perturbations can be calculated analytically, the gravitational collapse and subsequent hierarchical build-up of structure is a highly nonlinear process that can be followed only through numerical simulations. It has been shown by previous numerical studies (e.g., Jenkins et al. 2001; Sheth & Tormen 2002; Springel & Hernquist 2003b), and more recently by the state-of-the-art *Millennium Simulation* by Springel et al. (2005c), that the PS formula underestimates the abundance of high-mass halos by up to an order of magnitude. Therefore, whether or not rare quasars such as J1148+5251 can form in the  $\Lambda$ CDM cosmology remains an open question and an important test of the theory.

To date, only a limited number of analytical or semi-analytic models have addressed the early formation of a  $10^9 M_{\odot}$  SMBH at  $z \sim 6$  (Haiman & Loeb 2001; Haiman 2004; Yoo & Miralda-Escudé 2004; Volonteri & Rees 2005). These approaches use merger trees of dark matter halos generated using the PS theory, and assume a black hole accretion rate at or above the Eddington limit. However, as discussed above, the PS–based approach may be inaccurate. Moreover, it is not clear whether sufficient physical conditions for such large accretion rates exist in quasar systems as the hydrodynamics of the large-scale gas flow and feedback from black holes have not been incorporated in earlier modeling.

It is believed that the growth of SMBHs is closely linked to galaxy formation (e.g., Magorrian et al. 1998; Ferrarese & Merritt 2000; Gebhardt et al. 2000; Graham et al. 2001; Tremaine et al. 2002; Marconi & Hunt 2003; Haiman 2004; Kazantzidis et al. 2005; Li et al. 2006a), and that the growth is self-regulated by feedback (e.g., Silk & Rees 1998; Haehnelt et al. 1998; Fabian 1999; King 2003; Wyithe & Loeb 2003; Di Matteo et al. 2005; Springel et al. 2005b; Sazonov et al. 2005; Murray et al. 2005; Wyithe & Loeb 2005). Remarkably, self-regulated models with SMBH feedback in the form of thermal energy coupled to the ambient gas have been demonstrated to successfully reproduce many observations of galaxies, including the  $M_{\text{BH}}-\sigma$  relation (Di Matteo et al. 2005; Robertson et al. 2006b), galaxy colors (Springel et al. 2005a; Hopkins et al. 2006c), X-ray gas emission (Cox et al. 2006b), elliptical kinematics (Cox et al. 2006c) and the fundamental plane (Robertson et al. 2006a), quasar properties (Hopkins et al. 2005d,a), luminosity functions (Hopkins et al. 2005b,c, 2006b), and populations (Hopkins et al. 2006a,e,d), and the luminosity function of low-level AGN (Hopkins & Hernquist 2006). Furthermore, these simulations of binary mergers identify a plausible, merger-driven formation mechanism for massive black holes and luminous quasars (e.g., Di Matteo et al. 2005; Hopkins et al. 2006a; Robertson et al. 2006b).

Here, we present a model that accounts for the SMBH growth, quasar activity and host galaxy properties of the most distant quasar known. In our scenario, the quasar and its host galaxy form in a massive halo that originates from a rare density peak in the standard  $\Lambda$ CDM paradigm, and they grow

hierarchically through multiple gas-rich mergers, supporting an average star formation rate of  $\sim 10^3 M_\odot \text{yr}^{-1}$  that peaks at  $z \sim 8.5$ . Once the progenitors undergo sufficient dynamical friction to coalesce, the multiple SMBHs from the progenitor galaxies merge and exponentially increase their mass and feedback energy via accretion. At  $z \approx 6.5$  when the SMBH mass exceeds  $10^9 M_\odot$ , black hole accretion drives a sufficiently energetic wind to clear obscuring material from the central regions of the system and powers an optically luminous quasar similar to J1148+5251. We have devised a set of novel multi-scale simulations, which include cosmological N-body calculations on large scales and hydrodynamic simulations of galaxy mergers on galactic scales, coupled with the self-regulated growth of SMBHs, enabling us to follow galaxy assembly and quasar formation at  $z \sim 6$ .

This paper is organized as follows. In § 2, we describe our computational methods and models, which includes a set of large scale cosmological N-body simulations, and hydrodynamical galaxy mergers along the merging history of the quasar halo. In § 3, we present the formation and evolution of the quasar and its host galaxy, including the assembly of the galaxy progenitors, star formation, and SMBH growth, as well as the SMBH–host correlations, and properties of the quasar such as luminosities and lifetimes. We discuss feedback from starburst-driven winds, quasar abundances for cosmological models with different parameters, the implication of black hole mergers, and galaxies in the epoch of reionization in § 4, and summarize in § 5.

## 2. METHODOLOGY

Rare, high-redshift quasars originate in highly overdense regions in the initial dark matter density distribution and grow through hierarchical mergers, as predicted by the  $\Lambda$ CDM theory. Simulations of high-redshift quasar formation must model a large cosmological volume to accommodate the low abundance of this population, have a large dynamic range to follow the hierarchical build-up of the quasar hosts, and include the hydrodynamics of the gas flows in galaxy mergers. The cutting-edge *Millennium Simulation* by Springel et al. (2005c) follows structure formation in a box with side length of  $500 h^{-1} \text{Mpc}$  using  $2160^3$  dark matter particles. It reproduces the large-scale galaxy distribution as observed (Springel et al. 2006), and identifies an early quasar halo candidate at  $z = 6.2$  which ends up in the richest cluster at the present day. However, even such a large dynamic range still falls short of being able to follow the formation and evolution of the rarest quasars observed at the highest redshifts. Moreover, in order to address the properties of quasars and host galaxies, gasdynamics and physical processes related to star formation and black hole growth must be included. To satisfy these requirements, we have performed a set of novel multi-scale simulations that enable us to resolve individual mergers on galactic scales and retain the context of large-scale structure formation, as well as the evolution of black holes and stars.

First, we perform a coarse dark matter simulation in a volume of  $1 h^{-3} \text{Gpc}^3$  designed to accommodate the low number density of  $z \approx 6$  quasars. The largest halo at  $z = 0$ , within which the descendants of early, luminous quasars are assumed to reside (Springel et al. 2005c), is then selected for resimulation with higher resolution using a multi-grid zoom-in technique developed by Gao et al. (2005). The merging history of the largest halo at  $z \sim 6$ , which has reached a

mass of  $\sim 5.4 \times 10^{12} h^{-1} M_\odot$  through 7 major (mass ratio  $< 5:1$ ) mergers between redshifts 14.4 and 6.5, is extracted. These major mergers are again re-simulated hydrodynamically using galaxy models scaled appropriately for redshift (Robertson et al. 2006b) and adjusted to account for mass accretion through minor mergers. The simulations include prescriptions for star formation (Springel & Hernquist 2003a), and for SMBH growth and feedback (Di Matteo et al. 2005; Springel et al. 2005b), as described below.

### 2.1. Code and Parameters

Our multi-scale simulations were performed using the parallel, N-body/Smoothed Particle Hydrodynamics (SPH) code GADGET2 developed by Springel (2005) that is well tested in a wide range of applications from large scale structure formation to star formation. For the computation of gravitational forces, the code uses the “TreePM” method (Xu 1995) that combines a “tree” algorithm (Barnes & Hut 1986) for short-range forces and a Fourier transform particle-mesh method (Hockney & Eastwood 1981) for long-range forces. The PM-method works efficiently in large scale cosmological simulations, while the tree-method provides accurate forces for the large dynamic range of galaxy merger simulations.

GADGET2 implements the entropy-conserving formulation of SPH (Springel & Hernquist 2002) with adaptive particle smoothing, as in Hernquist & Katz (1989). Radiative cooling and heating processes are calculated assuming collisional ionization equilibrium (Katz et al. 1996; Davé et al. 1999). Star formation is modeled in a multi-phase ISM, with a rate that follows the Schmidt-Kennicutt Law (Schmidt 1959; Kennicutt 1998). Feedback from supernovae is captured through a multi-phase model of the ISM by an effective equation of state for star-forming gas (Springel & Hernquist 2003a). A prescription for supermassive black hole growth and feedback is also included, where black holes are represented by collisionless “sink” particles that interact gravitationally with other components and accrete gas from their surroundings. The accretion rate is estimated from the local gas density and sound speed using a spherical Bondi-Hoyle (Bondi & Hoyle 1944; Bondi 1952) model that is limited by the Eddington rate. Feedback from black hole accretion is modeled as thermal energy injected into surrounding gas, as described in Springel et al. (2005b) and Di Matteo et al. (2005).

The simulations presented in this paper adopt the  $\Lambda$ CDM model with cosmological parameters chosen according to the first year Wilkinson Microwave Anisotropy Probe data (WMAP1, Spergel et al. 2003),  $(\Omega_m, \Omega_b, \Omega_\Lambda, h, n_s, \sigma_8) = (0.3, 0.04, 0.7, 0.7, 1, 0.9)$ . Here,  $\Omega_m$  is the total matter density in units of the critical density for closure,  $\rho_{\text{crit}} = 3H_0^2/(8\pi G)$ . Similarly,  $\Omega_b$  and  $\Omega_\Lambda$  denote the densities of baryons and dark energy at the present day. The Hubble constant is parameterized as  $H_0 = 100 h \text{ km s}^{-1} \text{ Mpc}^{-1}$ , while  $\sigma_8$  is the root-mean-squared linear mass fluctuation within a sphere of radius  $8 h^{-1} \text{ Mpc}$  extrapolated to  $z = 0$ . We have also done the same cosmological simulations with WMAP third year results (WMAP3, Spergel et al. 2006),  $(\Omega_m, \Omega_b, \Omega_\Lambda, h, n_s, \sigma_8) = (0.236, 0.042, 0.759, 0.732, 0.95, 0.74)$  for comparison.

### 2.2. Cosmological Simulations

The quasars at  $z \sim 6$  have an extremely low comoving space density,  $n \sim 10^{-9} \text{ Mpc}^{-3}$ , and are believed to reside in massive dark matter halos with  $M \gtrsim 10^{13} M_\odot$  (Fan et al. 2003).

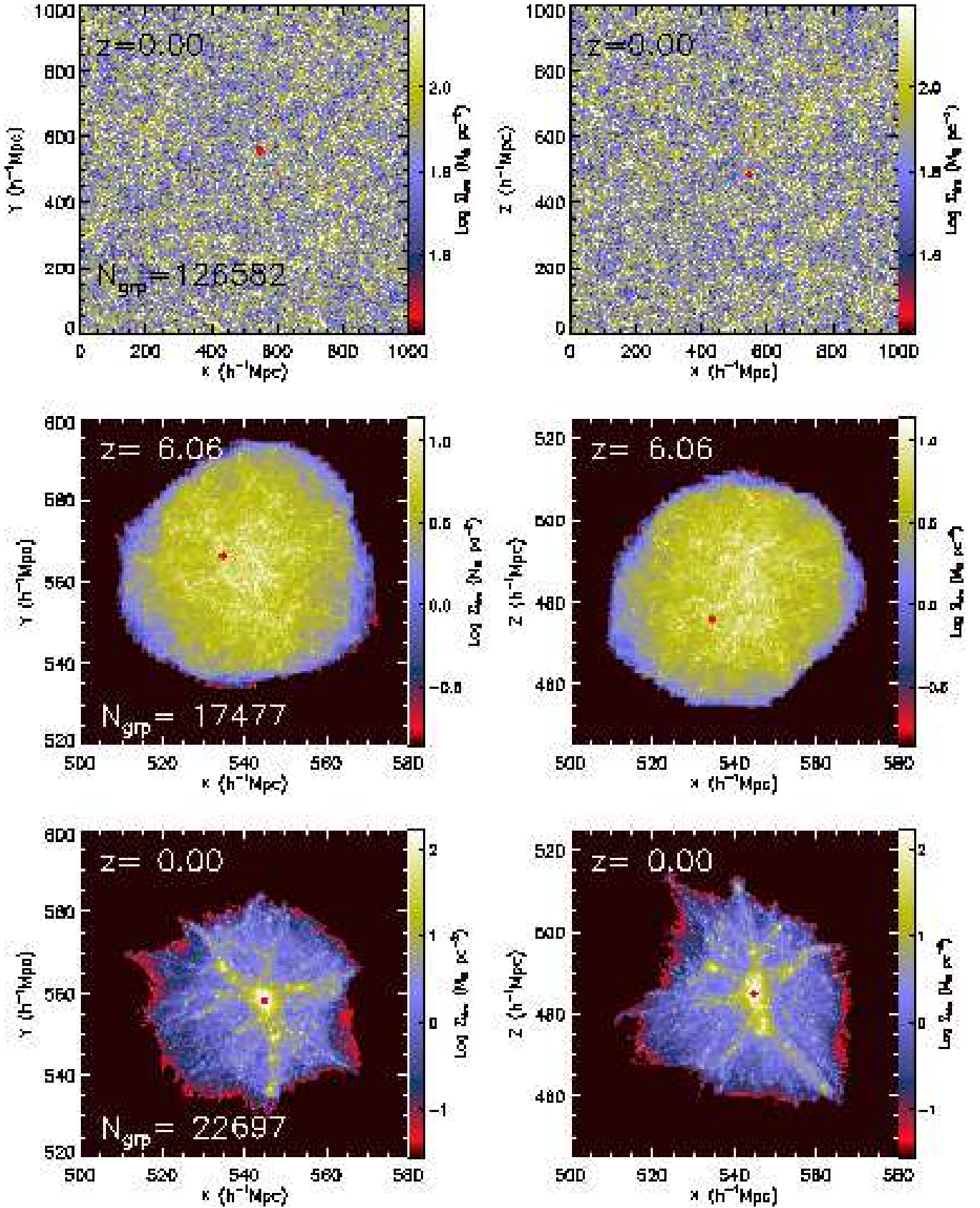


FIG. 1.— Snapshots from a cosmological simulation run with WMAP1 parameters. The images show projected density of dark matter in x-y (left column) and x-z (right column) planes, the red dot represents the center-of-mass of the quasar halo, which is the largest halo at both  $z = 0$  and  $z = 6$ . The top panels show the coarse run at  $z = 0$ . The middle and bottom panels show the zoom-in run at  $z = 6.06$  and  $z = 0$ , respectively, the number at the lower-left corner indicates the number of groups identified at that redshift.

Cosmological simulations of quasar formation must therefore model a volume of  $\sim 1 h^{-3} \text{Gpc}^3$  to account for the rarity of such objects. However, in order to resolve a  $10^{13} M_\odot$  halo at  $z \sim 6$  in a cosmological simulation with uniform resolution, a dark matter particle mass at least as small as  $10^{11} h^{-1} M_\odot$  and particle numbers of  $> 10^9$  are required. Tracking the merger history of such halos requires  $\sim 2$  orders of magnitude higher resolution and would be computationally prohibitive with standard techniques.

We achieve the mass resolution requirements for the merger history of a  $10^{13} M_\odot$  halo at  $z \sim 6$  by means of a two-step re-simulation. First, coarse dark matter cosmological simulations are performed to identify a candidate halo for the quasar host. A cubic volume  $L_{\text{box}} = 1 h^{-1} \text{Gpc}$  on a side is simulated with  $400^3$  particles, achieving mass and force resolutions of  $m_{\text{dm}} \sim 1.3 \times 10^{12} h^{-1} M_\odot$  and  $\epsilon \sim 125 h^{-1} \text{kpc}$  (comoving), respectively. To generate the initial conditions, we use the Boltzmann code CMBFAST by Seljak & Zaldarriaga (1996) to compute a linear theory power spectrum for our chosen cosmology. A random realization of the power spectrum is constructed in Fourier space, sampling modes in a sphere up to the Nyquist frequency of the mesh. The particle distribution is evolved forward in time to  $z = 0$  from its initial displacement at  $z = 30$  determined using the Zel'dovich approximation.

At the end of the simulation, halos are identified using a ‘‘friends-of-friends’’ (FOF) group-finding algorithm (Davis et al. 1985) with a fixed comoving linking length equal to 0.2 times the mean dark matter interparticle separation and a minimum of 32 particles per group (Springel & Hernquist 2003b). The mean overdensity of the groups corresponds approximately to the expected density of virialized halos (Springel et al. 2005c). From the more than 126000 groups identified in the  $1 h^{-3} \text{Gpc}^3$  volume at  $z = 0$  the largest halo with  $M(z = 0) \simeq 3.6 \times 10^{15} h^{-1} M_\odot$  is selected as a candidate halo for modeling the formation of a quasar at  $z = 6.5$ .

A multi-grid technique developed by Gao et al. (2005) and Power et al. (2003) is used to ‘‘zoom in’’ with high resolution on the selected halo region which has an effective side length of  $L_{\text{box}} \sim 50 h^{-1} \text{Mpc}$ . Large-scale tidal forces are captured by binning exterior particles into cells according to their distance from the high-resolution region. To ensure proper treatment of small-scale structure, the initial displacements of the high resolution particles are calculated assuming a higher initial redshift of  $z = 69$  and normalized to  $\sigma_8$  at  $z = 0$ . The re-simulation uses  $\approx 350^3$  particles, with  $\approx 340^3$  particles inside the high-resolution region. With this technique, the mass resolution increases by almost four orders of magnitude to  $m_{\text{dm}} \sim 2.8 \times 10^8 h^{-1} M_\odot$  while the spatial resolution reaches  $\epsilon \sim 5 h^{-1} \text{kpc}$ .

Figure 1 shows snapshots of both the coarse and high-resolution zoom-in runs that locate the quasar halo candidate. In the coarse run, the ‘‘cosmic web’’ is clearly seen, although the distribution appears nearly homogeneous on such large scales. In the zoom-in run, filamentary structures are prominent. Dark matter collapses along the filaments, and the largest halo forms in the deepest potential wells at the intersections of the filaments. The high resolution of the zoom-in run enables the identification of more halos with lower masses both at  $z = 0$  and at high redshifts as early as  $z \sim 17$ , which is sufficient to identify the halo progenitors of the candidate quasar at  $z \sim 6$ . It appears that the halo progenitor of the

largest one at the present day is also the most massive halo at  $z \sim 6$ , when it reaches a mass of  $M \approx 5.4 \times 10^{12} h^{-1} M_\odot$ , making it a plausible candidate for hosting a rare  $z \sim 6.4$  quasar.

### 2.3. Halo Mass Functions with Different Cosmological Parameters

The impact that variations in the cosmological parameters can have on large-scale structure formation can be understood from the theoretical mass function of halos, as derived by Press & Schechter (1974) and later developed by Lacey & Cole (1993). The comoving number density  $dn$  of halos of mass between  $M$  and  $M + dM$  can be described as,

$$\frac{dn}{dM} = \sqrt{\frac{2}{\pi}} \frac{\rho_0}{M^2} \frac{\delta_c(z)}{\sigma(M)} \left| \frac{d \ln \sigma}{d \ln M} \right| \exp \left[ -\frac{\delta_c(z)^2}{2\sigma^2(M)} \right], \quad (1)$$

where  $\rho_0$  is the local mean mass density,  $\delta_c(z)$  is the critical density of collapse at redshift  $z$  linearly extrapolated to the present day, and  $\sigma(M)$  is the mass variance, which is a function of the power spectrum  $P(k)$  with wavenumber  $k$  and the window function  $w(k)$ ,  $\sigma^2(M) = \frac{1}{2\pi^2} \int_0^\infty P(k) w^2(k) d^3k$ . The abundance of halos depends on the two functions  $\sigma(M)$  and  $\delta_{\text{crit}}(z)$ , each of which involves the cosmological parameters, in particular  $\sigma_8$ ,  $\Omega_m$  and  $\Omega_\Lambda$ . These parameters determine the formation epoch of a halo and its mass.

The recently-released third year WMAP3 results (Spergel et al. 2006) have lower values of  $\sigma_8$ ,  $n_s$  and  $\Omega_m$ , compared to WMAP1 (Spergel et al. 2003). The smaller  $\sigma_8$  from WMAP3 would lower the amplitude of the power spectrum, which in turn reduces  $\sigma(M)$ . Furthermore, a smaller  $\Omega_m$  would reduce  $\delta_c(z)$  and hence delay halo formation. So, compared to WMAP1, at a given redshift the WMAP3 parameters would yield a lower abundance of halos with mass  $M_{\text{halo}} \gtrsim M_*$ , where  $M_*$  is the halo mass corresponding to the characteristic luminosity in the Schechter luminosity function for galaxies (Schechter 1976); while for  $M_{\text{halo}} < M_*$ , it predicts a slightly larger halo abundance.

To test the sensitivity of our model to the new WMAP results, we have performed the same set of cosmological simulations with parameters from the WMAP3 measurements (Spergel et al. 2006). We find that indeed the changes implied by the new parameters primarily affect the formation time and the mass of the candidate quasar halo. For the same random phases in the initial conditions, the location of the most massive halo at  $z = 0$  remains the same in both the WMAP1 and WMAP3 runs, except that its mass is reduced by a factor of  $\sim 1.6$  for the WMAP3 parameters. Similarly, the mass of the largest halo at  $z \approx 6$  is altered by roughly the same factor. Other notable changes include: (1) the formation epoch of the first halo is shifted from  $z \sim 16.8$  in the WMAP1 run to  $z \sim 14.4$  in the WMAP3 run, and (2) the merging history of the largest halo at  $z \sim 6$  moves to lower redshifts in the WMAP3 run, but the number of major mergers remains the same.

Figure 2 shows the halo mass functions from different cosmological simulations. The PS mass function (Press & Schechter 1974), as well as the one corrected to match numerical simulations by Sheth & Tormen (2002) (ST), are also shown for comparison. One important feature in this figure is that the coarse runs agree well with the ST mass function, but show a larger comoving density at the high mass end than that predicted by the PS theory. Our results show that the PS formula underestimates the abundance of high-mass halos by nearly an order of magnitude at  $z = 0$ , and the

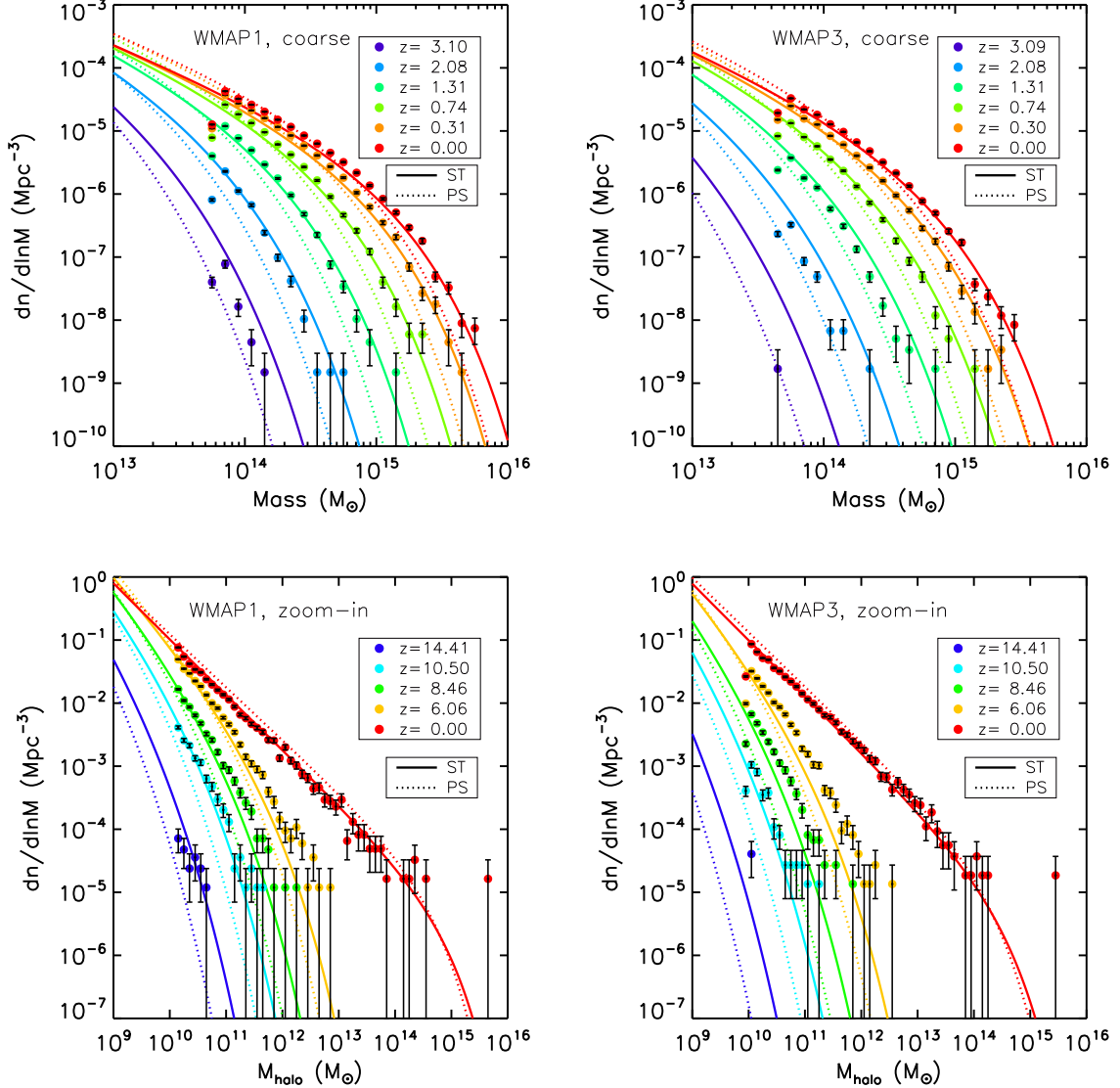


FIG. 2.— Halo mass functions from cosmological simulations with parameters from WMAP1 (*left*) and WMAP3 (*right*), respectively, and with different levels of resolution corresponding to our coarse (*top panels*) and zoom-in (*bottom panels*) runs. The colored symbols indicate different redshifts, while the error bar shows the Poisson error  $\sqrt{N}$ . The mass functions from Press & Schechter (1974) (PS, dotted line) and Sheth & Tormen (2002) (ST, solid line) are also shown for comparison. Please note that in the bottom panels, the analytical curves (ST and PS) apply only to a *random* region, they are not suitable for a highly overdense region where the most massive halos reside in the zoom-in box. So the high-mass end of the simulated mass function deviates significantly from the prediction, see text for more discussion.

discrepancy between the PS calculation and numerical simulations becomes larger at higher redshifts, confirming previous findings (e.g., Jenkins et al. 2001; Sheth & Tormen 2002; Springel & Hernquist 2003b; Springel et al. 2005c). This may explain why previous models using the PS formula to study the abundance of luminous quasars, which presumably form in massive halos, under-predicted the number of bright quasars at  $z > 5$  (e.g., Efstathiou & Rees 1988). Furthermore, these results also suggest that the commonly used analytical merger tree generated using the PS formula may not be suitable to study quasar formation at high redshifts.

There are two clear “shifts” of the mass function caused by resolution and cosmological parameters. Those from runs with higher resolution extend to higher redshifts, and at the same redshift, the WMAP1 runs produce more massive halos than the WMAP3 ones. As shown in Figure 2, the coarse runs produce mass functions only up to  $z \approx 3$  owing to limited mass

resolution, while the zoom-in runs can produce quite reasonable mass functions as early as  $z \approx 14$ . Because the zoom-in runs were deliberately centered on the highest density peak of the  $1 h^{-3} \text{Gpc}^3$  box, they each contain a very massive halo ( $M > 10^{15} M_{\odot}$  at  $z = 0$ ) by construction. This explains why the highest mass bin (which contains only one halo in this case) is  $\sim 2$  orders of magnitude larger than the theoretical curves (ST, PS), which apply only to a *random* region that has a much lower density fluctuation.

To summarize, at a given redshift, runs with the WMAP3 parameters yield slightly less massive halos than ones performed with the WMAP1 values. Or, to put it differently, objects in the WMAP3 cosmology will have masses similar to those for WMAP1, but at slightly later times (i.e. lower redshifts). In what follows, we are primarily concerned with investigating the plausibility of forming  $z \sim 6$  quasars through the self-regulated growth of SMBHs in hierarchical mergers,

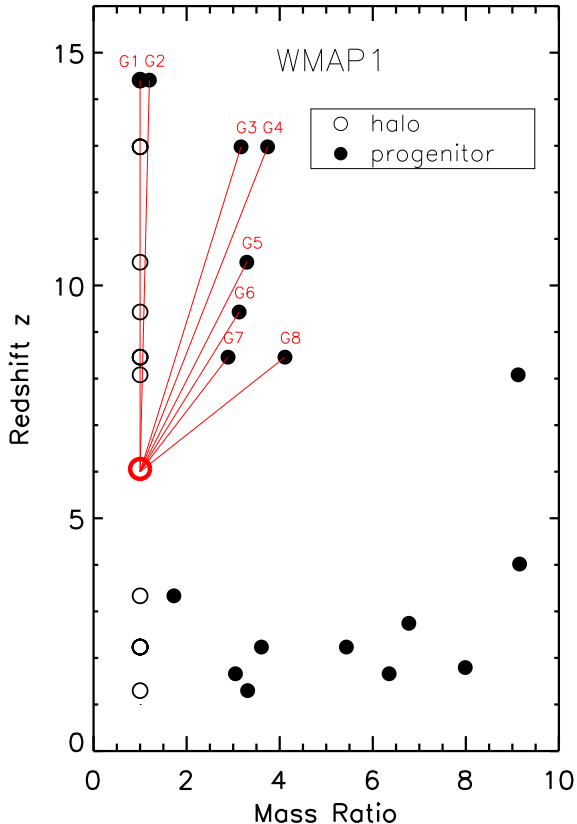


FIG. 3.— Schematic merging history of the largest halo at  $z=0$  traced by mergers at different redshifts with mass ratio  $\leq 10:1$ , which is defined as the mass ratio between the halo and progenitor at a given time. Each of the progenitors joins in this big merging event at a given redshift, interacts with the system, and subsequently merges with others at later times. The quasar host at  $z \sim 6$  is built up by seven successive major mergers of progenitors G1, G2, ... G8 from  $z \sim 14.4$  to  $z \sim 6.0$ , as illustrated by the red lines in this plot. The first interaction between G1 and G2 takes place at  $z \sim 14.4$ , then G3 and G4 join in the system at  $z \sim 13$ , followed by G5, G6, G7 and G8 at later times (see text for more details). The timeline of these events, the mass and other properties of these progenitors are listed in Table 1.

rather than precisely reproducing the properties of an individual quasar at a given redshift, such as J1148+5251. Most of our results are therefore based on runs with the WMAP1 parameters, to ease comparison with previous numerical work. If it were firmly established that e.g.  $\sigma_8$  is in reality smaller than its WMAP1 value, then a more exact match to a particular quasar could presumably be obtained by considering larger simulation volumes and identifying a suitable candidate host that is slightly rarer than the one we have chosen to focus on here.

#### 2.4. Merger Tree Construction

To follow the hierarchical mass assembly of the host galaxy over cosmic time, the merger tree of the halo is extracted from the cosmological simulation. This tree provides key information for computing the physical properties of the progenitor galaxy population. While the merger history of the halo includes a spectrum of progenitor masses, the most massive progenitors contribute the majority of the halo mass over the redshift range considered. We trace the merger history of the most massive progenitor at each redshift by using particle tags

to identify progenitor systems at earlier redshifts in the simulation. Groups that contribute at least 10% of the halo mass at a given time step are considered as the progenitors of the halo and are recorded. The procedure is repeated until the last progenitor is reached, producing the merging history.

Figure 3 illustrates the merging history of the largest halo at  $z=0$  in our cosmological simulation, which has a mass of  $\simeq 3.6 \times 10^{15} h^{-1} M_\odot$ . It is also the largest one at  $z \sim 6$  with a mass of  $\simeq 5.4 \times 10^{12} h^{-1} M_\odot$ . This schematic plot outlines the redshift of merger event, and the mass ratio of the halo to its galaxy progenitors at a given time. It shows that this halo grows rapidly through hierarchical mergers early on, with seven major mergers (mass ratio of the merging pairs  $\leq 5:1$ ) from  $z \sim 14.4$  to  $z \sim 8.5$  that build up a substantial fraction of the halo mass at  $z \sim 6$ .

In modeling the development of a  $z \sim 6$  quasar, we are primarily interested in “major” mergers, where the mass ratio of the merging galaxies is not too far from unity, for several reasons. First, it is believed that major mergers play the most important role in the formation and evolution of massive galaxies (e.g., Sanders & Mirabel 1996; Scoville et al. 2000; Veilleux et al. 2002; Conselice et al. 2003; Dasyra et al. 2006). Second, and of greater concern to us in this paper, in our picture for quasar fueling, gas in a rotationally supported disk loses angular momentum through gravitational torques excited by tidal forces in a merger, driving the growth of supermassive black holes. This process operates most effectively in a major merger because the tidal deformation of each galaxy is significant in such an event (Barnes & Hernquist 1991, 1992, 1996). Collisions involving galaxies with a mass ratio as large as  $10:1$  can induce gas inflows in disks (Hernquist 1989; Hernquist & Mihos 1995), but only for limited orbital configurations. For these reasons, we focus on mergers from the merger tree having a mass ratio  $\leq 5:1$ , as outlined by the red color in Figure 3.

In the resimulation of the merger tree as described in § 2.5, we take into account mass accretion of the halo by adding mass proportionally to each of the eight progenitor galaxies in the major mergers. This approach preserves the progenitor mass ratios and approximately preserves the dynamics of the major mergers (Dubinski 1998).

#### 2.5. Simulations of Galaxy Mergers Along the Tree

In order to model the formation and evolution, and properties of the quasar candidate, the merger tree is then resimulated hydrodynamically with galaxy models that consist of an extended dark matter halo, a rotationally supported, exponential disk of gas and stars and a central supermassive black hole. We follow the evolution of the system built up by seven major mergers hierarchically from  $z \sim 14.4$  to  $z \sim 6$ , as shown in Figure 3. Technically, this is a series of successive merger simulations. The first simulation includes G1 and G2 interacting at  $z \sim 14.4$ . It stops at  $z \sim 13$  and a new galaxy G3 is added into the system. During this process, all the dynamical properties of the pre-existing system (e.g. G1 and G2 in this case) are preserved, while G3 is added based on its properties and orbital parameters derived from cosmological simulations. Then a second merger simulation with G1, G2 and G3 starts. Such a procedure is repeated until all the progenitors enter the system. In the end, the simulation includes all eight galaxies. Eventually all these galaxies and black holes merge together. The duration of each merger simulation is determined by the merger tree. The redshift at which

TABLE 1  
PROGENITOR PROPERTIES AND NUMERICAL PARAMETERS

Galaxy <sup>a</sup>	$z^b$	$M_{\text{vir}}^c$ [ $10^{10} h^{-1} M_{\odot}$ ]	$V_{\text{vir}}^d$ [ $\text{km s}^{-1}$ ]	$f_{\text{gas}}^e$	$M_{\text{BH}}^f$ [ $10^5 h^{-1} M_{\odot}$ ]	$R_p^g$ [ $h^{-1} \text{kpc}$ ]	$R_0^h$ [ $h^{-1} \text{kpc}$ ]
G1	14.4	6.3	234.1	1.0	0.15	—	—
G2	14.4	5.3	220.3	1.0	0.15	0.2	7.1
G3	13.0	15.0	297.8	1.0	0.51	0.2	8.5
G4	13.0	17.7	314.6	1.0	0.51	0.3	10.7
G5	10.5	49.1	401.0	1.0	6.56	0.4	11.3
G6	9.4	79.6	448.6	0.9	23.3	0.5	18.2
G7	8.5	160.0	540.4	0.9	89.2	0.7	25.2
G8	8.5	207.7	589.5	0.9	89.2	1.0	34.5

<sup>a</sup> Name of galaxy progenitor. G1 is the halo at  $z = 14.4$ .

<sup>b</sup> Redshift at which the progenitor enters the merger tree.

<sup>c</sup> Virial mass, assuming overdensity  $\Delta = 200$ .

<sup>d</sup> Virial velocity, assuming overdensity  $\Delta = 200$ .

<sup>e</sup> Gas fraction of the progenitor baryonic mass.

<sup>f</sup> Progenitor black hole mass at the merger redshift.

<sup>g</sup> Pericentric distance of the incoming progenitor to the center-of-mass of the existing system.

<sup>h</sup> Initial distance of the incoming progenitor to the existing system.

each progenitor galaxy enters the merger tree, the properties of each progenitor galaxy, and the numerical parameters of the merger simulations are listed in Table 1. Below we describe the specification of these parameters.

### 2.5.1. Galaxy Models

The structure of the galaxy models is motivated from leading theories of dissipational disk galaxy formation in CDM cosmologies that, as shown by Mo et al. (1998), are successful in reproducing the observed properties of both present-day disk galaxies and damped Ly $\alpha$  absorbers in quasar spectra at high redshift. The initial galaxy models are constructed in dynamical equilibrium using a well-tested method (Hernquist 1993; Springel & White 1999; Springel 2000; Springel et al. 2005b). A halo is identified with a virial mass  $M_{\text{vir}}$  and a virial radius  $R_{\text{vir}}$  within which the overdensity  $\Delta = \rho_0/\rho_{\text{crit}} = 200$ , where  $\rho_0$  and  $\rho_{\text{crit}}$  are the mean and critical density, respectively. The density profile of the dark matter halo follows a Hernquist profile (Hernquist 1990), scaled to match that found in cosmological simulations (Navarro et al. 1997), as described in Springel et al. (2005b):

$$\rho_{\text{H}}(r) = \frac{M_{\text{vir}}}{2\pi} \frac{a}{r(r+a)^3}, \quad (2)$$

where  $a$  is a parameter that relates the Hernquist (1990) profile parameters to the appropriate NFW halo scale-length  $R_s$  and concentration  $C_{\text{vir}}$  ( $C_{\text{vir}} = R_{\text{vir}}/R_s$ ),

$$a = R_s \sqrt{2[\ln(1 + C_{\text{vir}}) - C_{\text{vir}}/(1 + C_{\text{vir}})]}. \quad (3)$$

The exponential disk of stars and gas are then constructed as in Hernquist (1993) and Springel et al. (2005b). The properties of the galaxy, including the virial mass  $M_{\text{vir}}$ , virial radius  $R_{\text{vir}}$  and halo concentration  $C_{\text{vir}}$  are scaled appropriately with redshift, as described in Robertson et al. (2006b). In particular, for a progenitor with virial velocity  $V_{\text{vir}}$  at redshift  $z$ ,  $M_{\text{vir}}$  and  $R_{\text{vir}}$  are calculated following Mo et al. (1998), while  $C_{\text{vir}}$  is adopted from Bullock et al. (2001), as briefly outlined below:

$$M_{\text{vir}} = \frac{V_{\text{vir}}^3}{10GH(z)}, \quad (4)$$

$$R_{\text{vir}} = \frac{V_{\text{vir}}}{10H(z)}, \quad (5)$$

$$H(z) = H_0 [\Omega_{\Lambda} + (1 - \Omega_{\Lambda} - \Omega_{\text{m}})(1+z)^2 + \Omega_{\text{m}}(1+z)^3]^{1/2}, \quad (6)$$

$$C_{\text{vir}} = 9 \left[ \frac{M_{\text{vir}}}{M_0} \right]^{-0.13} (1+z)^{-1}. \quad (7)$$

where  $G$  is the gravitational constant, and  $M_0 \sim 8 \times 10^{12} h^{-1} M_{\odot}$  is the linear collapse mass at the present epoch.

We assume a baryon fraction of  $f_b = 0.15$  for these high-redshift galaxies based on the WMAP1 result (Spergel et al. 2003). The gas fraction of each progenitor is extrapolated from the results of semi-analytic models of galaxy formation (Somerville et al. 2001), with 100% gas disks at  $z \geq 10$  and 90% at  $10 > z \gtrsim 8$ . The multiphase ISM is envisioned to consist of cold clouds embedded in a hot, tenuous gas in pressure equilibrium. Stars form out of the cold clouds by gravitational instability (Li et al. 2005) with a rate that is proportional to the surface density of the gas (Schmidt 1959; Kennicutt 1998; Li et al. 2006b).

In the adopted ISM model for the gas, the equation of state (EOS) is controlled by a parameter  $q_{\text{EOS}}$  that linearly interpolates between isothermal gas ( $q_{\text{EOS}} = 0$ ) and a strongly pressurized multiphase ISM ( $q_{\text{EOS}} = 1$ ). This EOS describes the dynamics of star-forming gas and accounts for the consequences of stellar feedback on galactic scales, and enables us to construct equilibrium disk models even with large gas fractions (Robertson et al. 2004; Springel & Hernquist 2005). Supernova feedback is modeled through thermal energy input into surrounding gas and can help evaporate the cold clouds to replenish the hot phase. For the simulation presented here a value of  $q_{\text{EOS}} = 0.5$  is used, but test simulations using  $q_{\text{EOS}} = 0.25 - 1.0$  produce average star formation and black hole accretion rates that converge to within 15%.

### 2.5.2. Black Hole Accretion and Feedback

The supermassive black holes are represented by collisionless “sink” particles. They interact with other particles gravitationally, and accrete the gas. Accretion of gas onto the black



holes is modeled using a Bondi-Hoyle-Lyttleton parameterization (Bondi 1952; Bondi & Hoyle 1944; Hoyle & Lyttleton 1941), in which the black holes accrete spherically from a stationary, uniform distribution of gas, as described in Di Matteo et al. (2005) and Springel et al. (2005b):

$$\dot{M}_B = \frac{4\pi\alpha G^2 M_{BH}^2 \rho}{(c_s^2 + v^2)^{3/2}}, \quad (8)$$

where  $M_{BH}$  is the black hole mass,  $\rho$  and  $c_s$  are the density and sound speed of the gas, respectively,  $\alpha$  is a dimensionless parameter of order unity, and  $v$  is the velocity of the black hole relative to the gas.

We assume the accretion has an upper limit by the Eddington rate,

$$\dot{M}_{Edd} \equiv \frac{4\pi G M_{BH} m_p}{\epsilon_r \sigma_T c}. \quad (9)$$

where  $m_p$  is the proton mass,  $\sigma_T$  is the Thomson cross-section, and  $\epsilon_r$  is the radiative efficiency. The latter determines the conversion efficiency of mass accretion into energy released as radiated luminosity. We adopt a fixed value of  $\epsilon_r = 0.1$ , which is the mean value for radiatively efficient Shakura & Sunyaev (1973) accretion onto a Schwarzschild black hole. In the simulations, the accretion rate is then the minimum of these two rates,  $\dot{M}_{BH} = \min(\dot{M}_{Edd}, \dot{M}_B)$ .

The feedback from the black holes is associated with the mass accretion. We assume that a small fraction ( $\simeq 5\%$ ) of the radiated energy couples to the surrounding gas isotropically as feedback in form of thermal energy. This fraction is a free parameter, determined by matching the observed  $M_{BH}-\sigma$  relation (Di Matteo et al. 2005). For more discussions on this prescription, see Hopkins et al. (2006a). This feedback scheme self-regulates the growth of the black hole, and has been demonstrated to successfully reproduce many observed properties of elliptical galaxies, as mentioned earlier.

### 2.5.3. Black Hole Seeds

To grow a black hole up to  $10^9 M_\odot$  in less than 800 million years, a wide range in seed masses, from  $10 M_\odot$  to  $10^6 M_\odot$ , have been suggested (e.g., Carr et al. 1984; Loeb & Rasio 1994; Bromm & Loeb 2003; Haiman 2004; Yoo & Miralda-Escudé 2004; Volonteri & Rees 2005; Begelman et al. 2006). The formation of the black hole seeds remains an open question, and several scenarios have been proposed. In particular, Fryer et al. (2001) show that rapid collapse of massive PopIII stars due to pair instability could produce black hole of  $\sim 10^2 M_\odot$ ; Bromm & Loeb (2003) suggest that hot and dense gas clump may collapse monolithically to form a massive black hole of  $\sim 10^6 M_\odot$  in metal-free galaxies with a virial temperature of  $10^4$  K; while Begelman et al. (2006) propose that  $\sim 20 M_\odot$  black holes could form by direct collapse of self-gravitating gas due to global instabilities in protogalactic halos, they then grow to  $10^{4-6} M_\odot$  with super-Eddington accretion. We adopt the picture where black hole seeds are the remnants of the first stars (Abel et al. 2002; Bromm & Larson 2004; Tan & McKee 2004; Yoshida et al. 2006; Gao et al. 2006). The remnant black hole mass is currently uncertain and widely debated. Recent theory of PopIII star formation predicts a mass range of  $\sim 30-500 M_\odot$ , but there are two regimes where a SMBH could form, either  $\leq 100 M_\odot$  or  $\geq 260 M_\odot$  (Heger et al. 2003, see also Yoshida et al. 2006 for a recent discussion). We have tested

the seed mass in the range of  $100-300 M_\odot$  and find that the exponential growth of the black holes during the merger makes our results insensitive to the choice in that range. We therefore assume that the black hole seed starts with an initial mass of  $200 M_\odot$  after the collapse of the first star at  $z = 30$ .

These seed black holes then grow in the centers of  $\sim 10^6 M_\odot$  halo which contains a large amount of high density primordial gas, as current theories predict that only one star forms per such mini-halo. The dense gas in the central region provides abundant fuel for BH accretion. To account for their evolution before the major mergers take place, the black holes are assumed to grow at the Eddington rate until their host galaxies enter the simulated merger tree. Such an approximation is supported by the fact that the Eddington ratio in the simulations depends on the galaxy interaction and strength of the feedback from the black holes. In our simulations, most black holes grow at nearly the Eddington rate in the early stages of a galaxy interaction when the feedback is weak. However, when the interaction and the feedback become stronger, the Eddington ratios fluctuate by orders of magnitude. So a constant accretion rate at the Eddington limit is no longer appropriate, as we show below. Under this assumption, the first progenitor galaxies (G1 and G2) of the quasar host have black hole seeds of order  $2 \times 10^4 h^{-1} M_\odot$  by the time it enters the merger tree at  $z = 14.4$ . However, we should emphasize that this assumption serves only as an upper limit of the early growth of the black holes. Our results in the next sections imply that even if all the black hole seeds had a uniform mass of  $\sim 10^5 M_\odot$  when they enter the merger tree, it is still possible to build a massive one to  $10^9 M_\odot$  at  $z \sim 6.5$  through gas-rich mergers.

In our model, mergers are invoked in the formation of the most massive black holes of  $\gtrsim 10^7 M_\odot$  because that requires large supplies of gas. Early on, however, this may not be necessary to grow the black hole seeds from  $\sim 100 M_\odot$  to the  $\sim 10^5 M_\odot$  we start from, because the accretion rate is small so other gas fueling could be sufficient. As demonstrated in Hopkins & Hernquist (2006), faint AGNs could be fueled by stochastic accretion of cold gas that does not involve mergers. A similar process could go on in the black hole seeds left by the PopIII stars at very high redshifts. We should point out that in our simulations, it is necessary for galaxy progenitors in the merger tree to have reasonable massive black hole seeds ( $\sim 10^5 M_\odot$ ) initially in order to build a  $10^9 M_\odot$  black hole at  $z \sim 6.5$ . However, our results are insensitive to specific formation recipes of the seeds. The formation of seed black holes at high redshifts is a challenging problem, and some of the proposed scenarios mentioned above may indeed be necessary to make our seeds. However, currently there is no observation available to test these models.

In the picture we adopt in which the seeds come from the first stars, the early accretion may be complicated by the feedback from the stars. We note that recent studies by Johnson & Bromm (2006); Abel et al. (2006) and Yoshida et al. (2007) show that HII regions form around the first stars, and that the halo gas would be photo-ionized, photo-heated, and evacuated by the radiation feedback from the stars. Johnson & Bromm (2006) suggest that such feedback would deplete the gas in the central region, and would delay the black hole accretion by up to  $10^8$  yrs. However, this destruction effect depends sensitively on the lifetime of these massive stars, and more importantly on the environment which determines both the gas density profile and gas replen-

ish from inflow of the expelled gas or neighboring halos. In the simulations presented in Johnson & Bromm (2006), the box size is only  $100 h^{-1} \text{kpc}$ , too small to contain the large scale gravitational potential and the large wavelength density modes that drive gas infall, so the initial gas density is low and the destruction timescale is long in this case. However, the quasar halo in our simulation resides in the highest density peak in a volume of  $1 h^{-1} \text{Gpc}^3$ , where the halo potential and gas density, as well as the accretion rate are much higher (Gao et al. 2006). For a  $200 M_{\odot}$  black hole, the accretion rate at Eddington limit is only  $10^{-6} M_{\odot} \text{yr}^{-1}$ , which corresponds to the Bondi accretion of molecular gas with a typical temperature of  $\sim 100 \text{K}$  at density  $\sim 10^2 \text{cm}^{-3}$ , as implied from equation (8). Such a density requirement is satisfied with the initial conditions of our model. Therefore, the gas re-incorporation timescale in our case may be substantially shorter than that estimated in Johnson & Bromm (2006). We will investigate in a future project the growth and evolution of the early black holes after the death of the first stars in such a cosmological environment, using hydro-radiation simulations that include both radiative transfer and black hole accretion with ultra-high resolutions.

#### 2.5.4. Numerical Parameters of Merger Simulations

The merger tree contains eight galaxies engaging in seven major mergers at different times. For each merger event, the initial orbits of the incoming progenitors are set to be parabolic, consistent with the majority of the major mergers in our cosmological simulation and with previous findings (Khochfar & Burkert 2006). The orientation of each merging galaxy is selected randomly. The initial separation between each merging pair is set to  $R_0 = R_{\text{vir}}$ , where  $R_{\text{vir}}$  is the virial radius of the incoming system, while the pericentric distance is chosen as  $R_p = 0.5 R_d$ , where  $R_d$  is the radial disk scale length of the incoming system. We have tested different choices of  $R_p$  and orientations, and found that the impact of these parameters is minor because the orbital properties of the progenitors change rapidly through interactions with the multiple galaxies in the system.

Throughout the merger simulation, the mass and force resolutions are fixed for each particle type, and the total initial particle number of  $1.0 \times 10^6$  results in particle masses of  $m_h = 1.1 \times 10^7 h^{-1} M_{\odot}$  for the halo and  $m_{g,s} = 2.2 \times 10^6 h^{-1} M_{\odot}$  for both the gas and stars. The gravitational softening lengths are  $\epsilon_h = 60 h^{-1} \text{pc}$  for halo particles and  $\epsilon_{g,s} = 30 h^{-1} \text{pc}$  for both gas and stars. In the simulations, it is impossible to resolve individual stars, and the accretion radii of some small black holes are under-resolved. However, with the sub-resolution implementation in our models, we can calculate time-averaged rates of star formation and black hole accretion from the large-scale properties of the gas, which are well resolved in our simulations. Resolution studies of a single merger (Springel et al. 2005b) with particle numbers from  $1.6 \times 10^5$  to  $1.28 \times 10^7$  show that resolution affects some fine structures of the gas and the instantaneous growth rates of star and black holes, but the time-averaged properties of the system converge to within 20%.

#### 2.5.5. Halo Escape Velocity

In a galaxy merger with black holes, the black holes may merge into one, or may be ejected by gravitational recoil in the final stage. Their fate depends on the halo escape velocity  $V_{\text{esc}}$ . If the recoil velocity is larger than  $V_{\text{esc}}$ , then

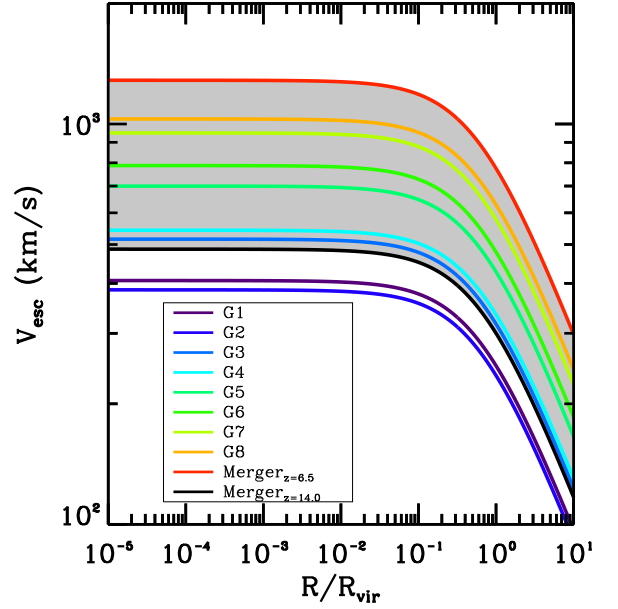


FIG. 4.— The halo escape velocity  $V_{\text{esc}}$  as a function of distance  $R/R_{\text{vir}}$  ( $R_{\text{vir}}$  is the virial radius) to the halo center for various models in our merger simulations. This plot includes the isolated halo progenitors G1 – G8 in Table 1, as well as the first merger remnant at  $z \simeq 14$  and the last one at  $z \simeq 6.5$ , as labeled in the legend. The shaded region indicates the range of the escape velocities of the mergers in our simulations, with the values in the central regions being  $486 \text{ km s}^{-1} \lesssim V_{\text{esc}} \lesssim 1284 \text{ km s}^{-1}$ .

the black hole will be kicked out of the halo. We follow Binney & Tremaine (1987) to calculate this important parameter  $V_{\text{esc}}$ . It is defined by

$$V_{\text{esc}}(r) = \sqrt{2|\Phi(r)|}, \quad (10)$$

where  $\Phi(r)$  is the gravitational potential at a given radius  $r$ . Because the halo is spherical, the potentials of different spherical shells add linearly, so  $\Phi(r)$  is contributed by two parts, i.e., shells within  $r$  ( $r' < r$ ) and outside ( $r' > r$ ):

$$\Phi(r) = -4\pi G \left[ \frac{1}{r} \int_0^r \rho_H(r') r'^2 dr' + \int_r^\infty \rho_H(r') r' dr' \right]. \quad (11)$$

where  $\rho_H(r)$  is again the Hernquist (1990) density profile of dark matter halo as in Equation 2.

Figure 4 shows the escape velocities of the halo progenitors G1 – G8 in Table 1, as well as two merger remnants at  $z \simeq 14$  and  $z \simeq 6.5$ , respectively. The escape velocity depends on the halo mass, redshift, and distance from the halo center. The  $V_{\text{esc}}$  remains constant in the central region, begins to decline around  $0.1 R_{\text{vir}}$ . At the center,  $V_{\text{esc}} \sim 2.5 V_{\text{vir}}$ , while at the virial radius  $R_{\text{vir}}$ , the escape velocity is comparable to the virial velocity (by a factor of  $\sim 1.5$ ). The isolated halo progenitors G1 – G8 have a  $V_{\text{esc}}$  range of  $\sim 385 - 1029 \text{ km s}^{-1}$ . The first merger halo at  $z \simeq 14$ , which has a mass of  $1.66 \times 10^{11} M_{\odot}$  as the merger of G1 and G2, has a central escape velocity of  $V_{\text{esc}} \sim 486 \text{ km s}^{-1}$ , while the final merger halo at  $z \simeq 6.5$ , which has a mass of  $7.7 \times 10^{12} M_{\odot}$ , has  $V_{\text{esc}} \sim 1284 \text{ km s}^{-1}$ . The shaded region indicates the range of the halo escape velocities of the mergers in our simulations. In particular, the escape speed in the halo central region has a

range of  $486 \text{ km s}^{-1} \lesssim V_{\text{esc}} \lesssim 1284 \text{ km s}^{-1}$ . This range is important for analysis of black hole ejection from gravitational recoil in the black hole binaries in § 3.4 and § 4.2.

### 3. FORMATION OF A LUMINOUS $Z \sim 6$ QUASAR

#### 3.1. Hierarchical Assembly of the Quasar Host

The vigorous merging history of the quasar host is illustrated through selected snapshots of the gas and stellar distributions in Figure 5 and Figure 6, respectively. The progenitors at high redshifts are very compact and gas rich. As the host galaxy of the quasar builds up hierarchically, strong gravitational interactions between the merging galaxies lead to tidal tails, strong shocks and efficient gas inflow that triggers large-scale starbursts, a phenomenon that has been demonstrated by many numerical simulations (e.g., Hernquist 1989; Hernquist & Katz 1989; Barnes & Hernquist 1991, 1996; Mihos & Hernquist 1994, 1996; Springel 2000; Barnes 2002; Naab & Burkert 2003; Li et al. 2004), as reviewed by Barnes & Hernquist (1992). The highly concentrated gas fuels rapid accretion onto the SMBHs (Di Matteo et al. 2005; Springel et al. 2005b). Between  $z \sim 14-9$ , the merging systems are physically small and the interactions occur on the scale of tens of kiloparsecs. By  $z \sim 9-7$ , when the last major mergers take place, the scale and strength of interactions have increased dramatically. Galaxies are largely disrupted in close encounters, tidal tails of gas and stars extend over hundreds of kiloparsecs, and intense bursts of star formation are triggered.

The black holes continue to grow rapidly during this period but are heavily obscured by a significant amount of circumnuclear gas. During galaxy mergers, the black holes follow their hosts to the center of the system and can interact closely with each other. It has been shown that black hole binaries decay rapidly in a gaseous environment and can merge within  $\sim 10^7$  yrs (Escala et al. 2004; Li 2007). Because the galaxies in our simulations are very gas rich and the gas is highly concentrated during the mergers, we therefore assume that the black holes merge efficiently owing to strong dynamical friction with the gas (Springel et al. 2005b). We will return to more discussions of this process in § 3.4 and § 4.2.

At redshift  $z \approx 6.5$  the progenitor galaxies coalesce, inducing high central gas densities that bring the SMBH accretion and feedback to a climax. The SMBH feedback then drives a powerful galactic wind that clears the obscuring material from the center of the system. The largest SMBH becomes visible as an optically-bright quasar (Hopkins et al. 2006a) during this phase, after which quasar feedback quenches star formation and self-regulates SMBH accretion. Consequently, both star formation and quasar activity die down, leaving a remnant which reddens rapidly, as illustrated schematically in Figure 6.

#### 3.2. Star Formation History

The evolution of the star formation rates (SFRs) of each individual galaxy, and total SFR of the whole system are shown in Figure 7 (*top panel*). The system forms stars rapidly as these compact and gas rich progenitors undergo strong interactions. The total SFR ranges from  $\sim 100 M_{\odot} \text{ yr}^{-1}$  to  $> 10^4 M_{\odot} \text{ yr}^{-1}$  between redshifts  $z \sim 9-8$  when the galaxies begin their final major mergers, while the SFRs of individual galaxies fall below a few  $\times 10^3 M_{\odot} \text{ yr}^{-1}$ , within the starburst intensity limit of  $10^3 M_{\odot} \text{ yr}^{-1} \text{ kpc}^{-2}$  proposed by Meurer et al. (1997) and Thompson et al. (2005). At  $z < 7$  the star formation rate decreases gradually owing to a depletion of the gas

supply and progressively stronger feedback from the SMBHs. At the time of final coalescence ( $z \approx 6.5$ ) the star formation rate is  $\sim 100 M_{\odot} \text{ yr}^{-1}$ , an order of magnitude lower than for estimates of J1148+5251 (Bertoldi et al. 2003a; Carilli et al. 2004). We note, however, that the estimates by these authors are based on the assumption that the FIR luminosity is dominated by young stars, and they cannot rule out the possibility that AGN may contribute significantly to the luminosity.

In a forthcoming paper (Li et al. 2007), we have calculated the infrared properties of the quasar system using a 3-D Monte Carlo radiative transfer code that incorporates adaptive grids and treats dust emission self-consistently. We find that the far-infrared luminosity of our quasar is not dominated by young stars but instead has a substantial quasar contribution of over 80%. This finding is supported by observations of J1148+5251 in near-IR (e.g., Charmandaris et al. 2004; Hines et al. 2006, and more recently Dwek 2006), which show a remarkably flat spectral energy distribution and suggest an AGN origin for the flux excess. Furthermore, adopting a total gas mass of  $\sim 10^{10} M_{\odot}$  (Walter et al. 2004; Narayanan et al. 2006c) in J1148+5251, a simple application of the Schmidt-Kennicutt star formation law (Schmidt 1959; Kennicutt 1998) gives a star formation rate of  $\sim 200 M_{\odot} \text{ yr}^{-1}$ , close to what we find here.

Within only about 600 Myrs from  $z = 14.4$  to  $z = 6.5$ , the system accumulates a stellar mass of  $\sim 10^{12} M_{\odot}$  as shown in Figure 7 (*bottom panel*). The specific star formation rate (SSFR), or “b-parameter” (e.g., Brinchmann et al. 2004), is defined as  $\text{SSFR} = \text{SFR}/M_{\text{star}}$ . It is a measure of the fraction of the total stellar mass currently forming at a specific time. The SSFR is typically larger in high-redshift galaxies than in ones at low redshifts owing to vigorous star formation. During the past several years, there has been rapid progress in observing galaxies at  $z \gtrsim 6$  using the *Hubble Space Telescope* (HST), and the *Spitzer Space Telescope* (Spitzer) coupled with ground-based observatories (e.g., Dickinson et al. 2004; Bunker et al. 2004; Bouwens et al. 2004; Giavalisco et al. 2004; Egami et al. 2005; Eyles et al. 2005; Mobasher et al. 2005; Yan et al. 2005, 2006; Eyles et al. 2006), and hundreds of these distant objects have been detected. These frontier observations suggest that the Universe experienced rapid star formation during the redshift interval  $14 \gtrsim z \gtrsim 6$ , and the development of large stellar systems in the mass range of  $\sim 10^{10-11} M_{\odot}$ . In particular, several groups (Egami et al. 2005; Yan et al. 2006; Eyles et al. 2006) find SSFRs in the range of  $10^{-1}-10^2 \text{ Gyr}^{-1}$  in their observations, consistent with our simulations.

#### 3.3. Metal Enrichment

Rapid star formation in the quasar progenitors produces an abundant mass of heavy elements to enrich the ISM. Observations of J1148+5251 show solar metallicity in the system (Barth et al. 2003; Walter et al. 2003; Maiolino et al. 2005; Becker et al. 2006). Figure 8 shows the metallicity in our simulated quasar system at different times. Note that the dips and jumps in the curves owe to incoming new galaxies which bring in metal-poor pristine gas and newly-formed stars. The quasar host reaches solar metallicity as early as  $z \sim 12$ , and maintains similar levels to later times. The spatial distribution of metallicity from both gas and stars at the peak quasar phase at  $z \approx 6.5$  is shown in Figure 9. The metals are widely spread owing to outflow from the quasar feedback and gas infall toward the merger center. The metallicity in the central region

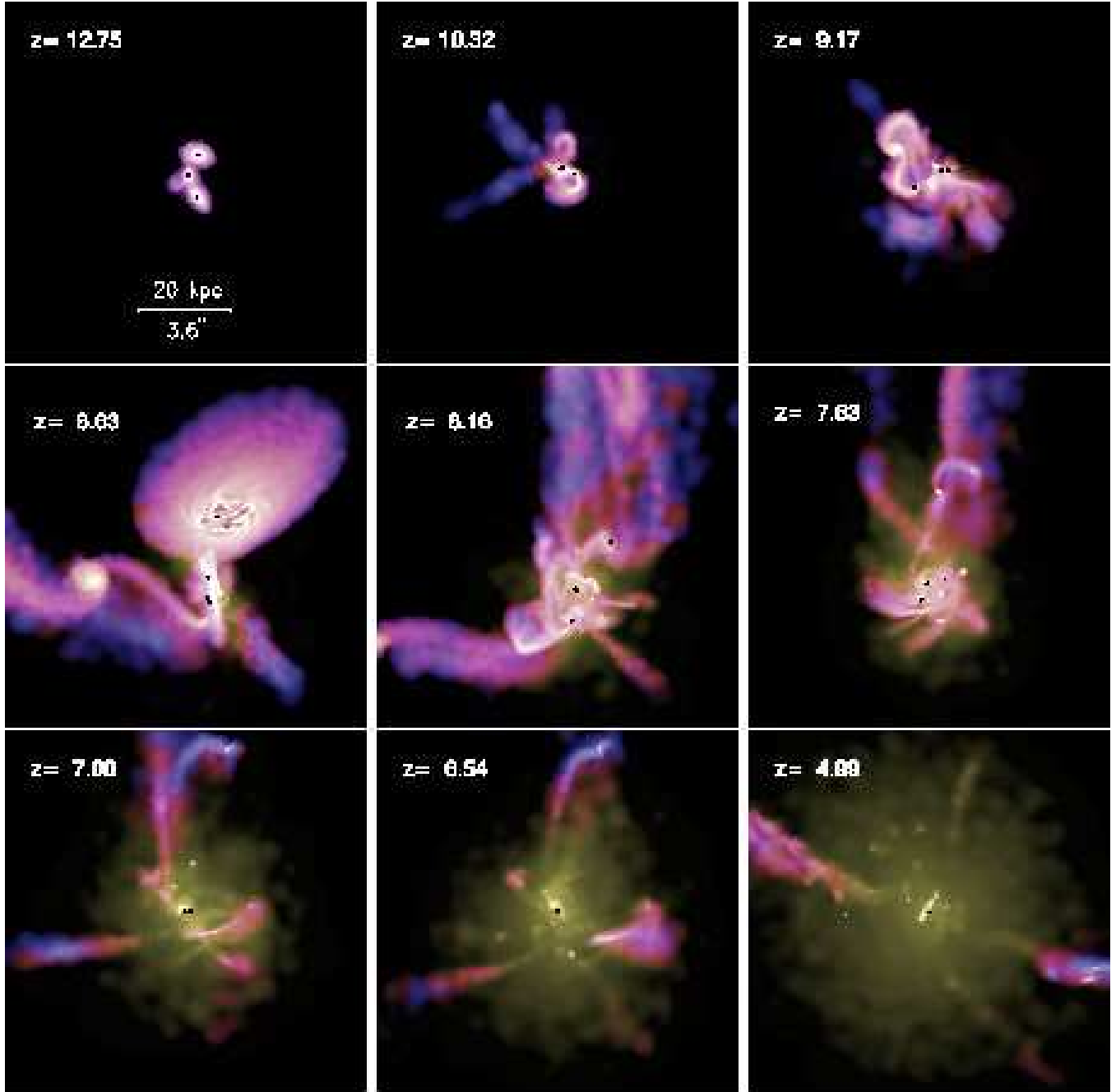


FIG. 5.— History of the quasar host shown in selected snapshots. The images give the projected gas density, color-coded by temperature (blue indicates cold gas, yellow indicates hot, tenuous gas). The black dots represent black holes. There are eight galaxies in total, engaging in seven major mergers along the timeline of the merger events as listed in Table 1. *Top panels* show interactions in the early stage from  $z \sim 13$  to 9. *Middle panels* show the last major mergers between  $z \sim 9$ –7, and *bottom panels* show the final phase. All the galaxies coalesce at  $z \approx 6.5$ , creating an extremely luminous, optically visible quasar (see Figure 6). At this time, there are three black holes, but the luminosity is dominated by the most massive one, which is more than two orders of magnitude larger than the others. These black holes merge into a single one at later time. The scale bar indicates a size of 20 kpc (comoving), corresponding to an angular size of  $3.6''$  at redshift  $z = 6.5$ .

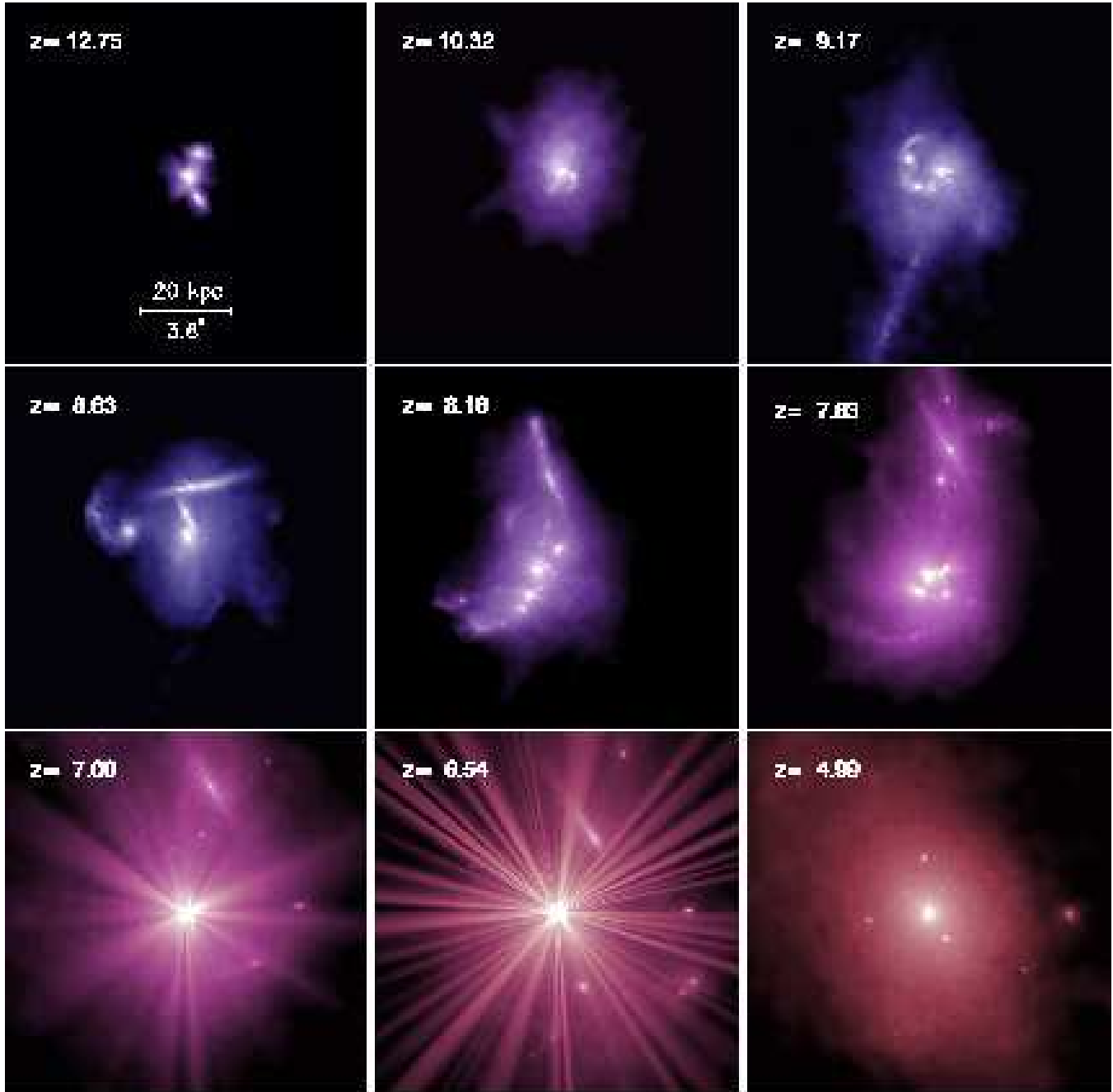


FIG. 6.— Same as Figure 5, but here the images show the projected stellar density, color-coded by the specific star formation rate (star formation rate per unit stellar mass). Blue indicates massive star formation in the galaxies, while red indicates little star formation. To illustrate the quasar activity, we have generated “rays” around the quasar. The number and strength of the rays are proportional to the bolometric luminosity of the black holes. These rays are artificial and serve only as a visual guide. The systems in *top panels* are blue, small and perturbed. The quasars appear very faint and buried. In the *middle panels*, strong interactions between galaxies boost star formation and black hole accretion, creating highly irregular morphologies and extremely blue galaxies. The quasars are heavily obscured by dense gas. At a later stage (*bottom panels*), feedback from the black holes quenches star formation, allowing the galaxy color to redden. The quasar becomes optically visible as strong outflows blow out the gas. It has a maximum luminosity around  $z \approx 6.5$  when all the galaxies coalesce. After that, both the quasar activity and star formation gradually die down, leaving behind an aging stellar spheroid.

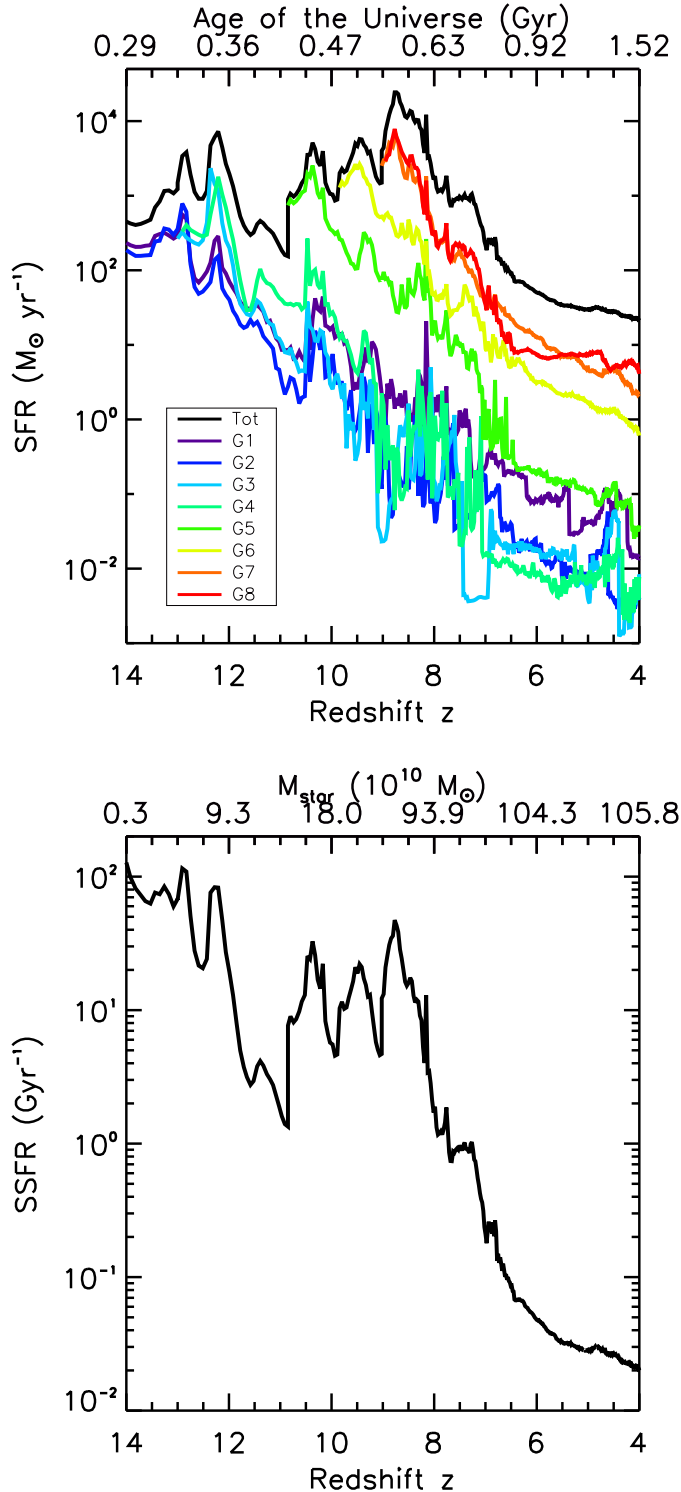


FIG. 7.— Time evolution of star formation rate (SFR, *top panel*) and specific star formation rate (SSFR, *bottom panel*), respectively. The colored lines indicate individual galaxies, while the black lines give summed quantities for the entire system.

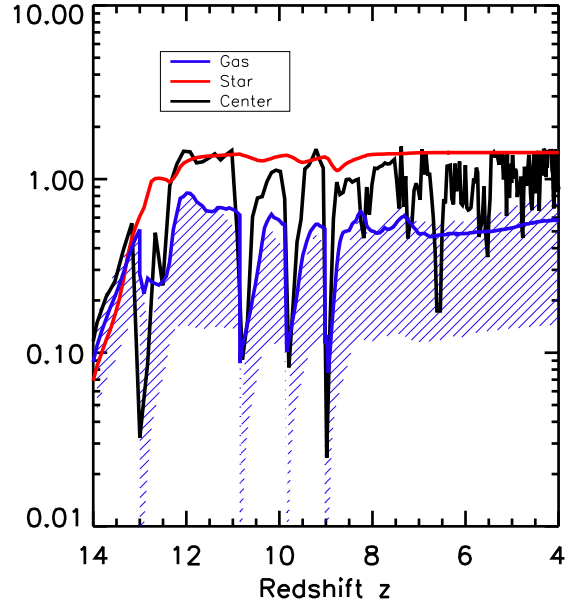


FIG. 8.— Time evolution of mass-weighted metallicity in the quasar host, from gas (blue curve), stars (red curve), and the mean value in the central region ( $R < 1$  kpc) of each galaxy (black curve). The blue hatched region indicates the range of 25%–75% of the gas metallicity.

of the merger remnant is slightly above the solar value. In some outer regions, because the gas and stars are still falling back to the system center, the infalling material triggers small-scale bursts of star formation. So the metallicity in these blobs appears to be super-solar, as shown in Figure 9.

Calculations of carbon monoxide emission using non-local thermodynamic equilibrium radiative transfer codes (Narayanan et al. 2006a,b) by Narayanan et al. (2006c) show CO luminosities, excitation patterns, and morphologies within the central  $\sim 2$  kpc of the quasar host center that are consistent with observations of J1148+5251 (Walter et al. 2003; Bertoldi et al. 2003b; Walter et al. 2004). These results were derived using Galactic CO abundances, and thus support our conclusions that significant metal enrichment takes place early in the quasar host, as a result of strong star formation in the progenitors.

#### 3.4. Growth of Supermassive Black Holes

In the simulations, the quasar host at  $z \sim 6$  is built up by eight progenitors, each containing a black hole in the center. Figure 10 shows the evolution of the black hole accretion rate, the Eddington ratio, and the integrated masses of the whole system and individual black holes. The total black hole accretion rate grows steadily during the hierarchical assembly of the host galaxy and peaks at  $\sim 10 M_{\odot} \text{ yr}^{-1}$  around  $z \approx 6.5$  during the final coalescence.

The Eddington ratio,  $L_{\text{bol}}/L_{\text{Edd}}$ , of each individual black hole varies with time, depending on the galaxy interaction and feedback from the black holes. The black holes maintain accretion at the Eddington limit for only a fraction ( $< 50\%$ ) of the time. At the peak of quasar activity, the Eddington ratio of the most massive black hole is near unity, while that of the other black hole is only 0.1. However, collectively, the whole system appears to accrete at  $L_{\text{bol}}/L_{\text{Edd}} \sim 1$  at  $z \gtrsim 6.5$ ,

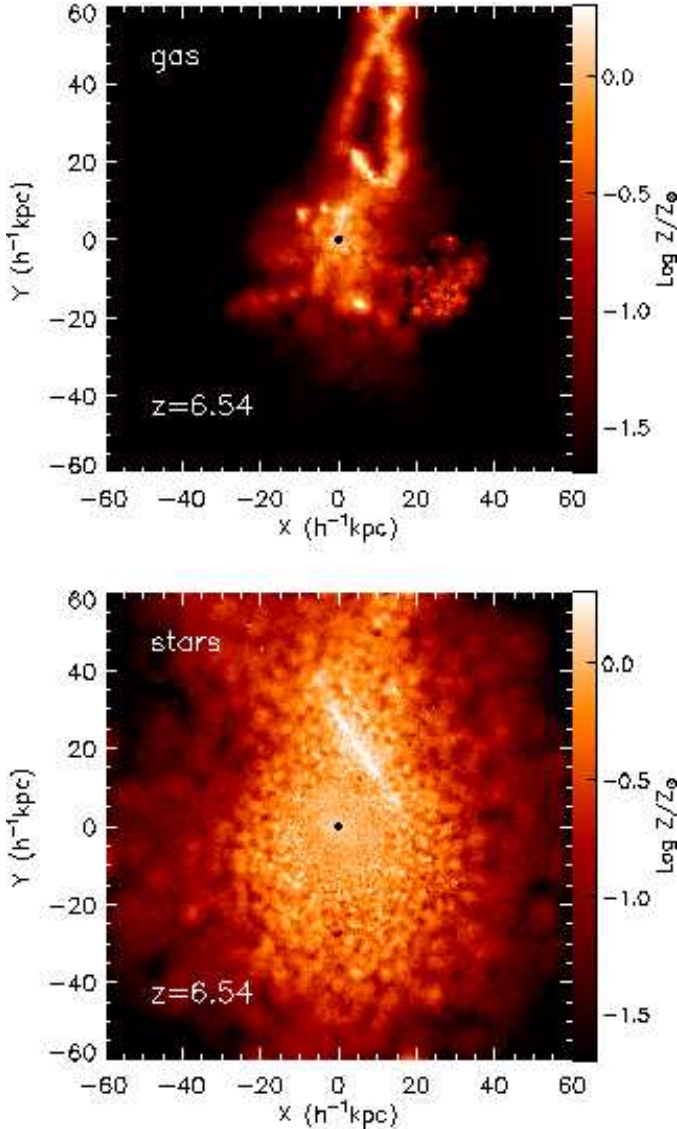


FIG. 9.— Spatial distribution of mass-weighted metallicity of the quasar host at  $z \approx 6.5$ , from both gas (*top panel*) and stars (*bottom panel*), respectively. The images are projected metallicity adaptively smoothed over 32 particles (analog to the SPH kernel in a 2-dimensional plane). The black dot indicates the center of the quasar.

as implied in Figure 10. Studies of black hole accretion (e.g., Vestergaard 2004; Kollmeier et al. 2005; Vestergaard & Fan 2006) show that the Eddington ratio has a wide range of 0.01–1.0, and it varies with both luminosity and redshift. Luminous systems tend to have higher  $L_{\text{bol}}/L_{\text{Edd}}$  than less-luminous counterparts, and at  $z \gtrsim 4$ , most quasars shine at nearly Eddington luminosity. Our results suggest that *individual* black holes do not always necessarily accrete at the Eddington rate. However, since high-redshift, luminous quasars may form through mergers of several galaxy progenitors containing black holes as in our case, therefore the growth of the quasar represents a *collective* contribution from each individual black hole. The total black hole mass increases from  $\sim 6 \times 10^4 M_{\odot}$  at  $z \approx 14$  to about  $2 \times 10^9 M_{\odot}$  at  $z \approx 6.5$ , close to that estimated for J1148+5251 by Willott et al. (2003) and Barth et al. (2003).

In the simulations, we do not have sufficient resolution nor

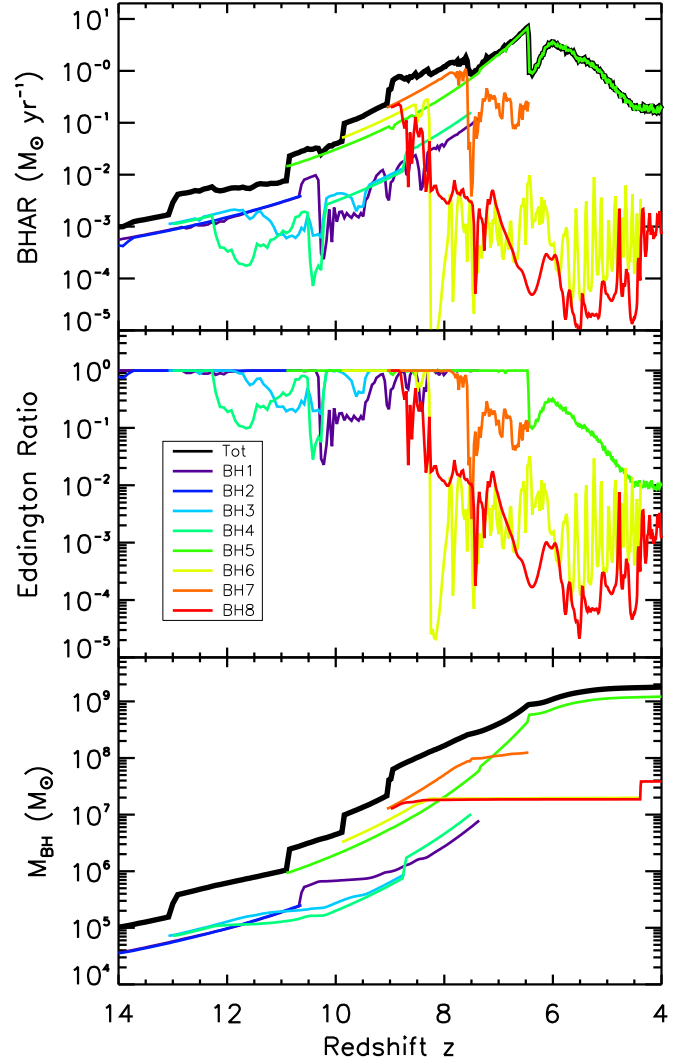


FIG. 10.— The growth history of the quasar system, including the black hole accretion rate BHAR, *top panel*, the Eddington ratio  $L_{\text{bol}}/L_{\text{Edd}}$  (*middle Panel*), and black hole mass (*bottom panel*). Note that the black curves represent totals, while colored curves show individual black holes, as indicated in the legend.

the relativistic physics to consider the ejection of black holes by gravitational recoil. The black holes are assumed to merge efficiently once their separation is below the spatial resolution. In the final stage of black hole mergers, the emission of gravitational wave carries linear momentum, which could cause the black holes to recoil (e.g., Bonnor & Rotenberg 1961; Peres 1962). If the recoil velocity is larger than the halo escape velocity, then the black holes will be kicked out from their halo (e.g., Fitchett 1983; Favata et al. 2004; Merritt et al. 2004; Madau & Quataert 2004; Haiman 2004; Yoo & Miralda-Escudé 2004; Volonteri & Rees 2005). Previous studies by (Haiman 2004; Yoo & Miralda-Escudé 2004; Volonteri & Rees 2005; Haiman 2006) suggest that constant or super-Eddington accretion is required to produce  $10^9 M_{\odot}$  black holes at  $z \sim 6$  if ejection of black holes is included. In particular, Haiman (2004) suggests a black hole will be ejected if the kick velocity  $V_{\text{kick}}$  for the coalescing SMBH binary is larger than twice the halo velocity dispersion  $\sigma_{\text{halo}}$ ,  $V_{\text{kick}} \gtrsim 2\sigma_{\text{halo}}$ , as the dynamical friction timescale for the

kicked black hole to return to the halo center is longer than the Hubble time (Madau & Quataert 2004). By applying this ejection criterion to a Press-Schechter merger tree of a  $8.5 \times 10^{12} M_{\odot}$  halo within which J1148+5251 is assumed to reside, Haiman (2004) finds that the SMBH of the quasar gains most of its mass rapidly from seed holes during  $17 \lesssim z \lesssim 18$  due to black hole ejection, and the SMBH likely accretes with super-Eddington rate in order to build a mass as that of J1148+5251.

However, the halo escape velocities or velocity dispersions in our model are much larger than the currently best estimates of the kick velocity. The quasar halo in our simulations has active merging history from redshifts  $z \simeq 14.4$  to  $z \simeq 6.5$ , and the halo progenitors have masses much higher than those considered in the previous studies (Haiman 2004; Yoo & Miralda-Escudé 2004; Volonteri & Rees 2005). The quasar halo builds its mass from  $\sim 1.16 \times 10^{11} M_{\odot}$  at  $z \simeq 14$  (the sum of progenitors G1 and G2 in Table 1) to  $7.7 \times 10^{12} M_{\odot}$  at  $z = 6.5$ . As shown in Figure 4 (the shaded region), the central escape velocity of the mergers in our simulations is in the range  $486 - 1284 \text{ km s}^{-1}$ . Currently, the maximum kick velocity for unequal-mass, non-rotating BH binary is in the range of  $\sim 74 - 250 \text{ km s}^{-1}$  from both analytic post-Newtonian approximation (e.g., Blanchet et al. 2005; Damour & Gopakumar 2006) and the ground-breaking full relativistic numerical simulations (e.g., Herrmann et al. 2006; Baker et al. 2006; Gonzalez et al. 2006). For equal-mass, spinning BH binary, Favata et al. (2004) estimate a range of  $\sim 100 - 200 \text{ km s}^{-1}$  using BH perturbation theory, and Herrmann et al. (2007) derive a formula from relativistic simulations,  $V_{\text{kick}} = 475S \text{ km s}^{-1}$ , where  $S \leq 1$  is the BH spin. This gives a maximum kick of  $475 \text{ km s}^{-1}$  for maximal spin. Although it is also reported that the recoil velocity can be as large as thousands  $\text{km s}^{-1}$  (Gonzalez et al. 2007; Campanelli et al. 2007) for BH binary in the orbital plane with opposite-directed spin. However, as pointed out by Bogdanovic et al. (2007), such a configuration is rather uncommon, especially in gas-rich galaxy mergers, because torques from accreting gas suffice to align the orbit and spins of both black holes with the large-scale gas flow. The resulting maximum kick velocity from such a configuration is  $< 200 \text{ km s}^{-1}$ . Overall, the kick velocity from the latest calculations of black hole binary is in the range of  $\sim 100 - 475 \text{ km s}^{-1}$ , falling safely below the escape velocities of the quasar halos in our simulations, so black hole ejection may be insignificant in our case.

Moreover, we find that our model can produce a  $10^9 M_{\odot}$  SMBH even if ejection is allowed. From Figure 10 (bottom panel), the  $10^9 M_{\odot}$  SMBH is dominated by BH5, most of its mass comes from gas accretion. Even if the less massive black holes, for example BH7 or BH8 was ejected, the most massive one BH5 is still able to reach  $\sim 10^9 M_{\odot}$  in the end. Furthermore, even if all the seeds started with  $\sim 10^5 M_{\odot}$  in the merger tree, the result would be about the same. We therefore conclude that the results from our modeling are robust. Supermassive black holes of  $\sim 10^9 M_{\odot}$  can grow rapidly through gas accretion and mergers hierarchically in the early Universe, constant or super-Eddington accretion is not necessary, unless the recoil velocity of the coalescing black hole binary is extremely high such that most of the black hole seeds in our simulations are ejected (e.g.,  $V_{\text{kick}} > 1000 \text{ km s}^{-1}$ ).

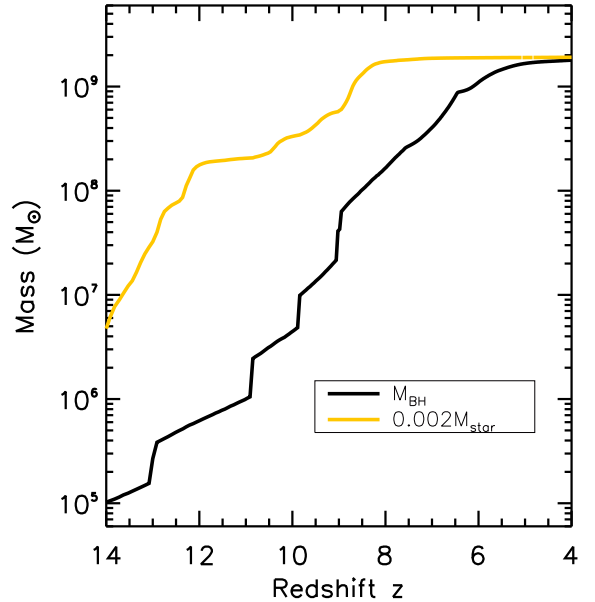


FIG. 11.— Evolution of total BH (black curve) and stellar (yellow curve) mass, respectively. The stellar mass is multiplied by a factor of 0.002, to reflect the observed correlation of  $M_{\text{BH}} \approx 0.002 M_{\text{star}}$  at the present day, as parameterized by Marconi & Hunt (2003).

### 3.5. Correlations between Supermassive Black Hole and Host Galaxy

Tight correlations between supermassive black holes and hosts have been observed in local galaxies (e.g., Magorrian et al. 1998; Ferrarese & Merritt 2000; Gebhardt et al. 2000), but the inference of these relationships at higher redshifts remains an open question. Because the eight galaxies in our system interact vigorously with each other, the stellar components are widely spread and mixed, it is impossible to separate individual galaxy-SMBH pairs, so we only consider the correlations in *total* quantity of the whole system. A comparison of the total stellar mass and total black hole mass is shown in Figure 11. At early time, both the stars and black holes grow rapidly through galaxy mergers. Shortly after the peak quasar phase, strong feedback suppresses both the accretion and star formation, the masses of the black holes and stars become saturated gradually, and in the end satisfy  $M_{\text{BH}} \approx 0.002 M_{\text{star}}$ , similar to the correlation measured in nearby galaxies (Magorrian et al. 1998; Marconi & Hunt 2003). Our results are consistent with findings by Robertson et al. (2006b) and Hopkins et al. (2007), and demonstrate that the observed  $M_{\text{BH}}-M_{\text{bulge}}$  scaling relation is a result of the coeval growth of the SMBH and its host galaxy, and that it holds across different cosmic times.

We note, however, that the velocity dispersion of the stars in the remnant center is about  $\sim 500 \text{ km s}^{-1}$  (after the system relaxes) owing to the deep potential well of the merger system, so the  $M_{\text{BH}}-\sigma$  relation falls below the correlation observed locally (Ferrarese & Merritt 2000; Gebhardt et al. 2000; Tremaine et al. 2002). Single mergers of progenitor galaxies constructed in a redshift range of  $z=0-6$  by Robertson et al. (2006b) appear to follow the observed  $M_{\text{BH}}-\sigma$  correlation with a weak redshift dependence



of the normalization, which results from an increasing velocity dispersion of the progenitors at higher redshift. The multiple mergers we derive from cosmological simulations take place at much higher redshifts and hence the progenitors have larger velocity dispersions, implying a larger deviation from the local  $M_{\text{BH}}-\sigma$  relation than in the work of Robertson et al. (2006b). However, because we do not follow subsequent mergers and accretion into the host halo below  $z \sim 6$ , the implications of this result for the evolution of the  $M_{\text{BH}}-\sigma$  relation are unclear.

Observations of active galaxies have yielded ambiguous results about the SMBH–spheroid relationship. For example, Greene & Ho (2006) report a lower zero-point of the  $M_{\text{BH}}-\sigma$  of local active galaxies than that of the inactive sample (Tremaine et al. 2002); at  $z > 0$ , Shields et al. (2003) found the same  $M_{\text{BH}}-\sigma$  relation in the redshift range  $z=1-3$ , while others (e.g., Treu et al. 2004; Walter et al. 2004; Borys et al. 2005; Peng et al. 2006; Shields et al. 2006) show correlations with various offsets. In particular, Walter et al. (2004) estimate a dynamical mass of  $\sim 5 \times 10^{10} M_{\odot}$  using the CO linewidth measured in J1148+5251, and suggest that the bulge is under-massive by at least one order of magnitude compared to the local  $M_{\text{BH}}-M_{\text{bulge}}$  relation. However, the CO calculation by Narayanan et al. (2006c) finds that the CO linewidth of the quasar in our simulation is larger than the mean 280  $\text{km s}^{-1}$  measured by Bertoldi et al. (2003b) and Walter et al. (2004) by almost an order of magnitude, and that the derived dynamical mass is  $\sim 10^{12} M_{\odot}$ , putting the simulated quasar on the  $M_{\text{BH}}-M_{\text{bulge}}$  correlation. Narayanan et al. (2006c) further suggest that the observed emission line may be sitting on top of a much broader line, which may be tested by future observations with large bandwidths.

The different relations reported from the observations may reflect a divergence of the methods used to estimate the black hole mass and stellar properties, or may represent different evolutionary stages of the systems (Wu 2006; Hopkins et al. 2007). More observations and better measurements of black hole mass and properties of host bulges will be crucial to study the SMBH–host relations in high-redshift quasar systems (Vestergaard & Peterson 2006) and to test our hypothesis.

### 3.6. Quasar Luminosities

Both the bolometric and attenuated luminosities of the quasar and the host galaxy in the simulations can be readily calculated following the methodology of Hopkins et al. (2005d). The bolometric luminosity  $L_{\text{bol}}$  of stars is calculated using the stellar population synthesis model of Bruzual & Charlot (2003), while that of a black hole is calculated as  $L_{\text{bol}} = \epsilon_r \dot{M} c^2$ , where  $\epsilon_r = 0.1$  is the radiative efficiency,  $\dot{M}$  is the black hole accretion rate, and  $c$  is the speed of light. In this calculation, the black holes are assumed to be non-rotating. If the black holes are spinning, their radiative efficiencies and luminosities would be higher due to the shrink of the innermost stable circular orbit, by up to a factor of 4 for maximal rotation.

The B-band luminosity of each source is corrected for attenuation by absorption from the ISM along the line-of-sight. We first calculate the line-of-sight column-density of the gas from each source to a distant observer. For each black hole we generate 1000 radial sight lines originating at the black hole particle location and uniformly spaced in the  $4\pi$  solid angle  $d\cos\theta d\phi$ , while for the stars, an accurate estimate of the

luminosity is possible with only one sight line per source owing to the extended distribution. Along each ray, the gas column density is calculated using a radial spacing of  $\Delta r = \eta h_{\text{sml}}$ , where  $\eta \leq 1$  and  $h_{\text{sml}}$  is the local SPH smoothing length. The distribution of line-of-sight properties converges for  $\gtrsim 100$  rays and at a distance of  $\gtrsim 100 \text{ kpc}$ . In the calculation, only the diffuse-phase density is considered because of its large volume filling factor  $\geq 99\%$ , allowing for a determination of the lower limit on the column density along a particular line of sight.

Adopting the mean observed intrinsic quasar continuum spectral energy distribution (Richards et al. 2006) gives a B-band luminosity which is well approximated by the following equation given by Marconi et al. (2004),  $\log(L_{\text{bol}}/L_{\text{B}}) = 0.80 - 0.067L + 0.017L^2 - 0.0023L^3$ , where  $L = \log(L_{\text{bol}}/L_{\odot}) - 12$ , and  $\lambda_{\text{B}} = 4400$ . We then use the Milky Way gas-to-dust ratio scaled by metallicity,  $A_{\text{B}}/N_{\text{H}} = (Z/0.02)(A_{\text{B}}/N_{\text{H}})_{\text{MW}}$  to determine the extinction along a given line of sight for this band. In the above calculation, we do not include a full treatment of radiative transfer, and therefore do not model scattering or re-processing of radiation by dust in the infrared. However, for the B-band luminosity, results using a 3-D Monte Carlo radiative transfer code are close to those calculated using the methods we present here (Li et al. 2007; Chakrabarti et al. 2006).

Figure 12 shows both the bolometric and attenuated B-band luminosities of the quasar, compared with observations of J1148+5251. The system is intrinsically bright with a total luminosity  $> 10^{11} L_{\odot}$ , and the host appears as an ultraluminous infrared galaxy (ULIRG) with  $L_{\text{bol}} > 10^{12} L_{\odot}$  for most of the time. At high redshifts,  $z > 8$ , starlight dominates the total luminosity. However, black holes take over at a later time. The quasar light-curve increases dramatically, peaking at  $z \approx 6.5$ , when it is powered by the most massive black hole accreting at near the Eddington rate. The estimated  $L_{\text{bol}}$  of J1148+5251 differs from that of the simulated quasar by less than the uncertainty in the luminosity estimate. The rest-frame B-band absolute magnitude reaches  $M_{\text{B}} \sim -26.5$ , almost one magnitude fainter than that of J1148+5251 derived from 1450 data (Fan et al. 2003). However, we should emphasize that in this paper, our main goal is to investigate the plausibility of forming luminous  $z \sim 6$  quasars through hierarchical mergers, rather than precisely reproducing the properties of an individual quasar such as J1148+5251, so the disagreement shown in Figure 12 should not be taken too literally. Moreover, the *exact* luminosity can change by a factor of several from relatively trivial or random details in the simulations. If the black hole spin is taken into account, then the simulated luminosities would increase by a factor of up to 4, which would match the observation of J1148+5251 better.

Feedback-driven outflows create un-obscured lines-of-sight, allowing the growing central SMBH to be visible as an optically-bright quasar between redshifts  $z \sim 7.5$  and  $z \sim 6.4$ . At the peak of the quasar activity, more than 50% of the 1000 sight lines have  $L_{\text{B}} \geq 10^{12} L_{\odot}$ . The absorbed light is re-emitted at infrared wavelengths by dust. We find that the luminosity in the far infrared (Li et al. 2007) is close to  $L_{\text{FIR}} \sim 10^{13} L_{\odot}$  estimated for J1148+5251 by Bertoldi et al. (2003a). Moreover, we find that up to 80% of the FIR light comes from the black hole, while stars contribute only  $\sim 20\%$ . This may explain why the star formation rate at  $z \approx 6.5$  during the peak quasar phase is an order of magnitude lower than the estimate from FIR observations (Bertoldi et al. 2003a), which will be contaminated by the AGN.

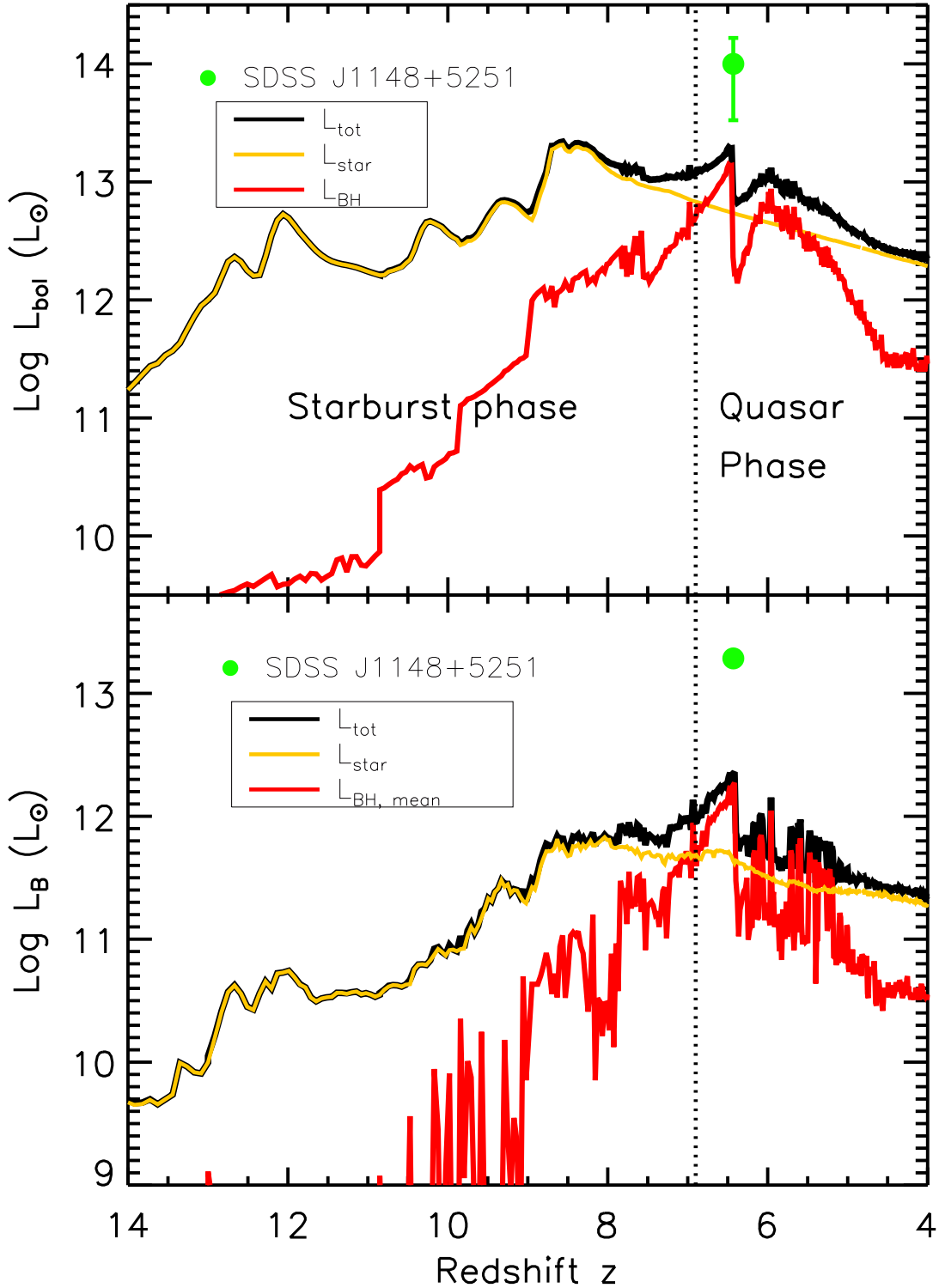


FIG. 12.— Comparison of luminosities from simulations and observations. Shown are bolometric (*top panel*) and attenuated luminosities in the rest-frame B-band (*bottom panel*). Note  $L_{\text{bol}}$  of SDSS J1148+5251 (green dot) is an estimate for a SMBH of  $3 \times 10^9 M_{\odot}$  accreting at the Eddington rate, with the error bar indicating the mass range of  $1\text{--}5 \times 10^9 M_{\odot}$  (Willott et al. 2003; Barth et al. 2003), while the  $L_{\text{B}}$  is converted from observations at wavelength 1450 (Fan et al. 2003). The yellow, red, and black curves represent luminosities of stars, black holes, and total (sum of the above two), respectively. For the black holes,  $L_{\text{BH,mean}}$  is the average luminosity over 1000 sight lines. Note in the luminosity calculation, the black holes are assumed to be non-rotating. If the black holes are rotating, their radiative luminosities could be higher by up to a factor of a few, see text for more discussions.

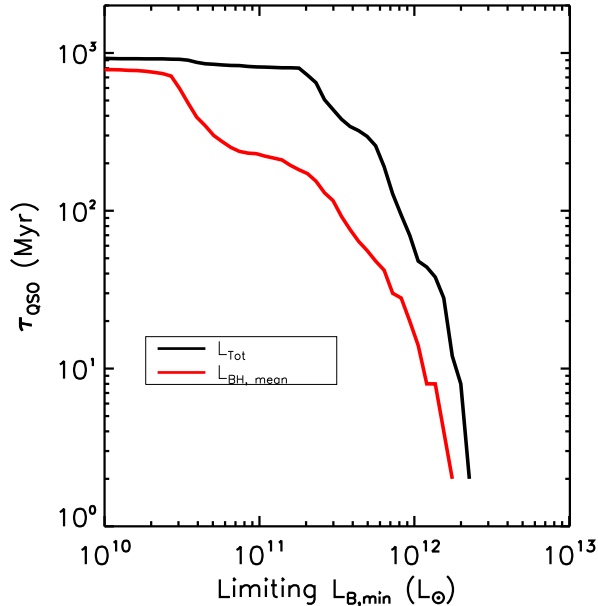


FIG. 13.— Quasar lifetimes as functions of different B-band limiting luminosities. The black and red curves represent the total luminosity of the system, and mean luminosity over 1000 sight lines of the black hole, respectively, corresponding to the curves of the same color in the bottom panel of Figure 12.

Another prominent feature of Figure 12 is a clear phase transition from starburst to quasar. It has long been suggested that ULIRGs are powered by starbursts in galaxy mergers (for reviews, see Sanders & Mirabel 1996; Jooe 2006), and that bright quasars are the descendants of ULIRGs (Sanders et al. 1988; Norman & Scoville 1988; Scoville 2003; Alexander et al. 2005). This conjecture has been supported by observations of quasar hosts (e.g., Stockton 1978; Heckman et al. 1984; Hutchings & Neff 1992; Bahcall et al. 1997; Hutchings 2005), and theoretical modeling (Hopkins et al. 2006a). In Li et al. (2007), we calculate the spectral energy distributions (SEDs) of the quasar system and its galaxy progenitors. We find that the SEDs of the system at  $z > 8$  are characterized by those of starburst galaxies (Sanders & Mirabel 1996), while at the peak quasar phase, the SEDs resemble those observed in  $z \sim 6$  quasars (Jiang et al. 2006). We also find that the system evolves from cold to warm ULIRG as it transforms from starburst to quasar phase. Our results provide further theoretical evidence for the ULIRG–quasar connection in quasar systems in the early Universe.

The quasar lifetimes depend on the observed luminosity threshold, as proposed by Hopkins et al. (2005d). In our simulation, at the peak luminosity of  $L_B \approx 2 \times 10^{12} L_\odot$ , the quasar lifetime is roughly  $\sim 2 \times 10^6$  yrs, as shown in Figure 13. Again, if black hole spin is included in the calculation, the luminosity of the quasar would increase by a factor of several, and the quasar lifetime would be longer. However, when increasing the radiative efficiency, the Salpeter time ( $e$ -folding time for Eddington-limited black hole growth, Salpeter 1964) is increased by an identical factor, meaning it would also require a longer time to reach the same mass. If high-redshift quasars are rapidly rotating, then, our calculations demand

that either the seeds be *much* more massive at  $z \gtrsim 6$ , or that they accrete in a super-Eddington manner. In other words, if the observed Sloan quasars at  $z \sim 6$  shine with Eddington luminosity but are rotating rapidly, then our model suggests that their masses would be considerably smaller than estimated.

We note that recent *Spitzer* observations by Jiang et al. (2006) show that 2 out of 13 quasars at  $z \sim 6$  have a remarkably low NIR-to-optical flux ratio compared to other quasars at different redshifts, and these authors suggest that the two quasars may have different dust properties. According to our model, however, these two outliers may be young quasars that have just experienced their first major starburst but have not yet reached peak quasar activity, so the light from star formation may be dominant, or comparable to that from the accreting SMBH still buried in dense gas. This may explain the low NIR flux, as well as the B-band luminosity and the narrow  $L_\alpha$  emission line, which are primarily produced by the starburst. We will address this question further in a future paper with detailed modeling and IR calculations (Li et al. 2007).

#### 4. DISCUSSION

##### 4.1. Comparison with Previous Models and Robustness of Our Results

Our multi-scale simulations that include large-scale cosmological N-body calculations and hydrodynamic simulations of galaxy mergers, as well as a self-regulated model for black hole growth, have successfully produced a luminous quasar at  $z \sim 6.5$  with a black hole mass of  $\sim 2 \times 10^9 h^{-1} M_\odot$  and a number of properties similar to those of J1148+5251, the most distant quasar detected at  $z = 6.42$  (Fan et al. 2003). Our approach differs from previous semi-analytic studies by Haiman & Loeb (2001); Haiman (2004); Yoo & Miralda-Escudé (2004); Volonteri & Rees (2005) and Volonteri & Rees (2006) in the following ways:

1. We use a realistic merger tree derived directly from multi-scale, high-resolution cosmological simulations. The previous studies used merger trees of dark matter halos generated with the extended Press-Schechter theory (Press & Schechter 1974; Lacey & Cole 1993), which may underestimate the abundance of high-mass halos by up to one order of magnitude, as shown in § 2.3. Also, the merger trees in those studies started from much higher redshifts than what we consider here. In our model, the quasar halo is the largest one in a volume of  $1 h^{-3} \text{Gpc}^3$ . It has a mass of  $\sim 7.7 \times 10^{12} M_\odot$  at  $z \sim 6.5$  built up through seven major mergers from  $z \simeq 14.4$  to  $z \simeq 6.5$ .
2. We follow the evolution of the system and treat the gas dynamics, star formation, and black hole growth properly. This approach is critical to investigation of the properties of both black holes and host galaxies, and their evolution (e.g., Di Matteo et al. 2005; Springel et al. 2005b; Robertson et al. 2006b; Hopkins et al. 2006a), but it was not included in those previous studies on formation of  $z \sim 6$  quasars.
3. We employ a self-regulated model for the growth of supermassive black holes, in which the accretion is regulated by the black hole feedback, and the rate is under the Eddington limit. In the previous studies, the black hole growth was unregulated, but instead a constant- or super-Eddington accretion rate was used.

4. In our simulations, we do not consider black hole ejection caused by gravitational recoil owing to insufficient resolution and lack of relativistic physics. However, the halo escape velocities in our simulations are in the range of  $486 - 1284 \text{ km s}^{-1}$ , much larger than the kick velocity  $\sim 100 - 475 \text{ km s}^{-1}$  (e.g., Herrmann et al. 2006; Baker et al. 2006; Gonzalez et al. 2006; Herrmann et al. 2007, see § 2.5.5 and § 3.4 for more details). Therefore, black hole ejection may be negligible in our case. Previous studies had much smaller halo progenitors at higher redshifts than ours, so the black hole seeds would be more likely subject to ejection from their halos. This leads to the conclusion in these studies that constant or super-Eddington accretion is needed owing to significant black hole ejection. Our results are robust within the best estimates currently available for the recoil velocity of the black hole binary.
5. The black hole seeds in the galaxy progenitors in our simulations are massive (e.g.,  $\sim 10^5 M_\odot$  at  $z \sim 14$ ). The sub-resolution recipe in our model does not allow us to resolve the actual formation and accretion of such black holes below this mass scale. The formation of these seeds is an unsolved problem, but our results do not depend on the specific prescription of the formation process. We adopt a picture in which the seed holes come from the remnants of the first stars (which have a mass  $200 M_\odot$  at  $z = 30$ ) and grow under Eddington limit until they enter the merger tree we simulated. If the growth is delayed by radiation feedback from the PopIII stars (e.g., Johnson & Bromm 2006), then super-Eddington accretion, or other proposed scenarios (e.g., Bromm & Loeb 2003; Begelman et al. 2006) may be necessary to form massive seeds of  $\sim 10^5 M_\odot$  in the protogalaxies.

Overall, we conclude that the results from our simulations, which are more realistic and more detailed than the models previously done, are robust. Supermassive black holes of  $\sim 10^9 M_\odot$  can form rapidly through gas-rich hierarchical mergers under Eddington limit, even within a short period of time. We find that constant or super-Eddington accretion is not necessary unless the above assumptions in our modeling break, i.e., there are no massive black hole seeds of  $10^5 M_\odot$  available at  $z \sim 14$ , or the recoil velocity of the coalescing black hole binary is extremely high (e.g.,  $> 1000 \text{ km s}^{-1}$ ). Under these extreme circumstances, some “exotic” processes such as super-Eddington accretion may be necessary to grow a  $\sim 10^9 M_\odot$  SMBH within a few hundred million years. However, we should note, as pointed out by Bogdanovic et al. (2007), that most gas-rich galaxy mergers have a configuration such that the orbit and spins of both black holes are aligned with the large-scale gas flow owing to torques from accreting gas. Such a configuration has a maximum kick velocity  $< 200 \text{ km s}^{-1}$ , which is well below the escape velocity of a  $10^{10} M_\odot$  dwarf galaxy, as well as those of the halos in our modeling.

#### 4.2. Merging History of Black Holes

During the galaxy mergers, the black holes follow their host halos to the system center and can form binaries (or multiple systems). The coalescence of a black hole binary in-

cludes three distinct phases: inspiral, merger, and ringdown (e.g., Flanagan & Hughes 1998). Whether black hole binaries can coalesce on short timescales is a matter of debate. In a stellar environment, it has been argued that a binary hardens very slowly owing to an eventual depletion of stars that cause the binary to lose angular momentum (e.g., Begelman et al. 1980; Milosavljević & Merritt 2003). In a gaseous environment, however, numerical simulations by Escala et al. (2004) and Li (2007) show that the binaries decay rapidly owing to strong dynamical friction with the gas, and they likely merge within  $10^7$  years. Because our galaxies are very gas rich and have large central concentrations of gas during the mergers, we assume the black hole particles coalesce once their separation decreases below our spatial resolution ( $30 h^{-1} \text{ pc}$ ) and their relative speed falls below the local gas sound speed (Springel et al. 2005b).

In the simulations, we do not have sufficient resolution nor the relativistic physics to consider the ejection of black holes by gravitational recoil during the merger phase. However, as discussed in § 2.5.5 and § 3.4, the halo escape velocities in our simulations are much larger than the maximum kick velocity for black hole binary estimated from the latest relativistic calculations. So black hole ejection is likely unimportant in our modeling. To accurately address gravitational recoil in the galaxy merger simulations, we need to include general relativity, resolve the dynamics of black hole binaries with extremely high resolution, and calculate the halo potential in a cosmological context (in which halo potential distribution may be different from that of a single object). However, such a comprehensive treatment is impossible at the moment. We therefore assume the black holes merge quickly once they reach the stage of gravitational radiation.

These coalescing supermassive black holes will be strong sources of gravitational radiation detectable by the Laser Interferometer Space Antenna (*LISA*, Folkner 1998), as suggested by many authors (e.g., Thorne & Braginskii 1976; Haehnel 1998; Flanagan & Hughes 1998; Menou et al. 2001; Hughes 2002; Sesana et al. 2005; Koushiappas & Zentner 2006). By tracing the merging history of the SMBHs, *LISA* could shed light on the distribution, structures and evolution of the associated dark matter halos. Because luminous, high-redshift quasars are likely sites of vigorous hierarchical mergers, they may be the best targets for *LISA* to explore the early Universe.

#### 4.3. Feedback from Starburst-driven Winds

Vigorous star formation would induce a galactic wind and mass outflow, a phenomenon that has been observed to prevail in both local star-forming galaxies as indicated by blueshifted optical absorption lines (e.g., Martin 1999; Heckman et al. 2000; Martin 2005; Rupke et al. 2002, 2005), and Lyman Break Galaxies at  $z \sim 3$  as indicated by blueshifted interstellar absorption lines and redshifted Ly $\alpha$  emission lines (e.g., Pettini et al. 2002; Shapley et al. 2003), as well as Ly $\alpha$  emitters at  $z \sim 5.7$  (Ajiki et al. 2002). These galactic winds are generally thought to play a significant role in galaxy evolution (e.g., see Veilleux et al. 2005 and Cox et al. 2006a for recent reviews).

The strong starburst preceding the major quasar phase in our simulations may drive strong galactic winds and affect the black hole growth. To investigate the impact of the feedback from a starburst-driven wind on the growth of the black hole, we have done the same merger simulation with lower resolu-

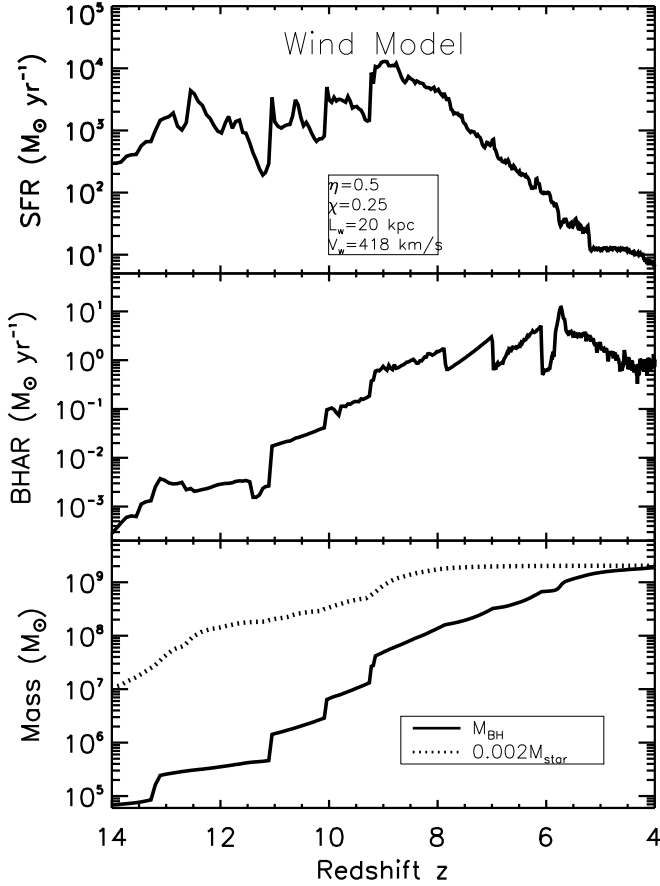


FIG. 14.— Evolution of star formation and black hole growth in merger simulations with a starburst-driven wind model. The simulation is run with lower resolution ( $N_{\text{tot}} \sim 5 \times 10^5$ ), and the specifications of the wind model is: wind efficiency  $\eta = 0.5$ , wind energy fraction  $\chi = 0.25$ , wind free travel length  $L_w = 20 \text{ kpc}$ , and a wind velocity  $V_w = 418 \text{ km s}^{-1}$ .

tion ( $N_{\text{tot}} \sim 5 \times 10^5$ ) and with a canonical wind model from Springel & Hernquist (2003b): the wind efficiency  $\eta = 0.5$ , which measures the coefficient of the star formation that determines the mass outflow; the energy fraction from supernovae injected into the wind  $\chi = 0.25$ , wind free travel length  $L_w = 20 \text{ kpc}$ , and a wind velocity  $V_w = 418 \text{ km s}^{-1}$ . As demonstrated by Cox et al. (2006a), this wind model is able to reproduce the starbursts as observed in Lyman Break Galaxies, and therefore is suitable to our study.

We find that the impact of the starburst-driven wind on the quasar evolution is minor, as shown in Figure 14. Both the histories of star formation and black hole growth remain roughly the same as in the simulation without a starburst wind, only the amplitude is lowered by a factor of  $\sim 1.5$ . Similarly, the final masses of the black hole and the stars are reduced by roughly the same factor, but the quasar host is still on the  $M_{\text{BH}}-M_{\text{bulge}}$  correlation. The peak quasar phase is delayed to  $z \sim 6$ . Overall, the starburst wind affects the gas dynamics locally, but owing to the deep potential of the system, its impact on the process of quasar formation is minor. Our results support the finding by Cox et al. (2006a) that feedback from starburst-driven winds alone is ineffective at regulating the growth of the central black hole, so feedback from the

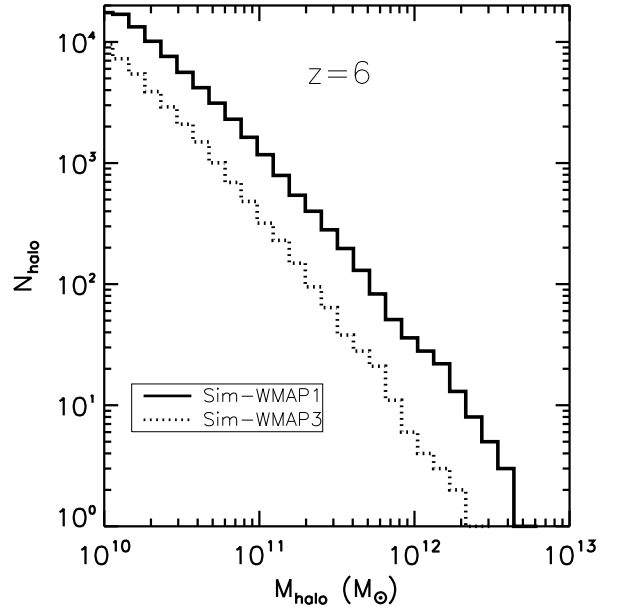


FIG. 15.— Comparison of halo abundances at  $z \sim 6$  from the zoom-in simulations with parameters from both WMAP1 (solid line) and WMAP3 (dashed line). The volume of the high-resolution zoom-in region is  $\sim 50^3 h^{-3} \text{ Mpc}^3$ .

black hole plays the dominant role in the formation and evolution of quasars.

#### 4.4. Abundance and Fate of Quasar Halos at $z \sim 6$

Because we have so far simulated only one quasar in a volume of  $1 h^{-3} \text{ Gpc}^3$ , we are not yet able to constrain the expected abundance of quasars  $z \sim 6$ . As mentioned in § 2.3, at a given redshift, cosmological simulations with parameters from WMAP1 produce more massive halos than runs with WMAP3 owing to a larger value of  $\sigma_8$ . Figure 15 shows the number of halos at  $z \sim 6$  from the zoom-in runs with parameters from both WMAP1 and WMAP3. There are about three dozen halos with mass  $M > 10^{12} M_{\odot}$  in the WMAP1 run, while in the WMAP3 run there are only a handful of such halos. However, since in our picture the quasar activity depends not only on the halo mass, but also on the merging history, an accurate estimate of the quasar abundance and luminosity function would require hydrodynamical simulations of all the quasar candidates in a large box, which are currently unavailable. Nevertheless, all conditions being equal, the change from the WMAP3 parameters would produce fewer luminous quasars at  $z \sim 6$ . This suggests that in a WMAP3 cosmology, the quasar observed with the largest redshift, J1148+5251, might have formed in a slightly higher overdensity peak than that we have presented here. In that event, if the WMAP3 determination of  $\sigma_8$  were correct, we would need to identify a rarer density fluctuation to match J1148+5251 at its observed redshift. However, this does not change our conclusion that the most distant and luminous quasars can form from hierarchical galaxy mergers in the  $\Lambda$ CDM cosmology.

Imaging surveys of J1148+5251 show that there is no other luminous quasar from the same epoch in the field (Carilli et al. 2004; White et al. 2005; Willott et al. 2005). In our simulations, around the peak of quasar activity at  $z \approx 6.5$ , there are no other halos of mass  $> 10^{12} M_{\odot}$  within a few Mpc of this

quasar. However, the numerous major mergers this halo experienced prior to the peak quasar activity demonstrates that this region was once highly clustered with massive halos, but they merged to become a bigger one by  $z = 6.5$ .

As seen from Figure 3, this quasar halo will undergo a handful of major mergers at a later time from  $z \sim 4-1$ , and eventually end up as a cD-like galaxy at the center of a rich cluster. Since we do not follow hydrodynamically the evolution of the quasar at  $z < 4$ , the physical conditions of these mergers remain undetermined. It is not clear whether this halo would experience more episodes of starburst or quasar activity later on during these mergers. Therefore, the final black hole mass and other properties of this quasar at the present day are deferred to future simulations that follow its evolution to  $z = 0$ .

#### 4.5. Galaxies in the Epoch of Reionization

The epoch of reionization (EoR) is an important landmark event in cosmic history that constrains the formation of the first luminous objects (Loeb & Barkana 2001). The recent results of WMAP3 indicate that the Universe was 50% reionized at  $z \approx 9.3$  (Page et al. 2006; Spergel et al. 2006), while studies of Gunn-Peterson absorption (Gunn & Peterson 1965) suggest that reionization began as early as  $z \sim 14$  and ended at  $z \sim 6$  (Fan et al. 2006). At present, it is believed that the reionization sources are star-forming galaxies since there are insufficient quasars at  $z > 6$  as indicated by the steep quasar luminosity function (Fan et al. 2006).

The galaxy progenitors of the quasar in our simulations underwent extreme and prolonged starbursts before  $z \sim 6.5$ . Less extreme galaxies in this epoch may also have vigorous star formation histories. Detecting these galaxies and determining their contribution to reionization will be crucial to understanding the EoR (Hernquist & Springel 2003; Barton et al. 2004; Davé et al. 2006). As reviewed by Hu & Cowie (2006), recent observations using both broad-band colors (e.g., Dickinson et al. 2004; Yan et al. 2005; Bunker et al. 2004; Bouwens et al. 2004; Giavalisco et al. 2004; Egami et al. 2005; Eyles et al. 2005; Mobasher et al. 2005; Yan et al. 2006; Eyles et al. 2006) and narrow-band Ly $\alpha$  emission (e.g., Hu et al. 2002; Malhotra & Rhoads 2004; Stern et al. 2005) have detected  $\sim 500$  galaxies at  $z \sim 6$  and a handful at  $z \gtrsim 7$  (Bouwens et al. 2005). The low luminosity density of galaxies currently detected at  $z > 7$  seems insufficient to reionize the Universe. However, ongoing surveys with the HST and Spitzer telescopes, and future missions such as the *Dark Ages z Ly $\alpha$  Explorer* (DAzLE, Horton et al. 2004) and the *James Webb Space Telescope* (JWST, Windhorst et al. 2006) will search deeper and further for high-redshift objects, and may eventually unveil ionizing sources in the EoR.

#### 5. SUMMARY

We have presented a model that accounts for the SMBH growth, quasar activity and host galaxy properties of the most distant quasar observed at  $z = 6.42$ , by following the hierarchical assembly of the quasar halo in the standard  $\Lambda$ CDM cosmology. We employ a set of multi-scale simulations that include large-scale cosmological N-body calculations and hydrodynamic simulations of galaxy mergers, and a recipe for black hole growth self-regulated by feedback. We first perform a coarse N-body simulation in a volume of  $1 h^{-3} \text{Gpc}^3$  to identify the largest halo at  $z = 0$ , which is assumed to be the descendant of the earliest luminous quasar. We then “zoom

in” on the halo and resimulate the region with higher resolution sufficient to extract its merging history starting from very high redshift. The largest halo at  $z \sim 6$  reaches a mass of  $\sim 5.4 \times 10^{12} h^{-1} M_{\odot}$  through 7 major mergers between  $z \sim 14.4-6.5$ . These major mergers are again re-simulated hydrodynamically using galaxy models and recipes for star formation, SMBH growth, and feedback.

We find that the quasar host galaxy builds up rapidly through gas-rich major mergers, with star formation rates up to  $10^4 M_{\odot} \text{yr}^{-1}$ , reaching a stellar mass of  $\sim 10^{12} M_{\odot}$  at  $z \sim 6.5$ . The black holes grow through gas accretion under the Eddington limit in a self-regulated manner owing to their own feedback. As the galaxies merge, the black holes coalesce to form a dominant black hole, reaching a peak accretion rate of  $\sim 20 M_{\odot} \text{yr}^{-1}$  and a mass of  $M_{\text{BH}} \sim 2 \times 10^9 M_{\odot}$  at  $z \sim 6.5$ . Feedback from black hole accretion clears away the obscuring gas from the central regions, making the quasar optically visible from  $z \sim 7.5-6$ . At the peak of the quasar phase, the star formation rate, metallicity, black hole mass, as well as quasar luminosities of the simulated system are consistent with observations of J1148+5251.

Our results demonstrate that rare and luminous quasars at high redshifts can form in the standard  $\Lambda$ CDM cosmology through hierarchical, gas-rich mergers, within the available cosmic time up to the early epoch of  $z \approx 6.5$ , without requiring exotic processes. Our model should also provide a viable formation mechanism for other distant, luminous quasars. Moreover, we predict that quasar hosts at high redshifts follow similar  $M_{\text{BH}}-M_{\text{bulge}}$  correlation observed locally as a result of the coeval evolution of the SMBHs and host galaxies. Better measurements of black hole masses and host properties with future observations will therefore be crucial to test our prediction. Furthermore, we predict that the progenitors of the distant quasars undergo strong and prolonged starbursts with rates  $\sim 10^3 M_{\odot} \text{yr}^{-1}$  at higher redshifts  $z > 8$ , that would contribute to the reionization of the Universe. Detecting these early galaxies and unveiling the epoch of reionization will be an important goal of current and future missions in observational cosmology.

We thank Volker Bromm, Romeel Davé, Suvendra Dutta, Zoltan Haiman, Scott Hughes, Adam Lidz, Chris McKee, Desika Narayanan, Hans-Walter Rix, Alice Shapley, Rachel Somerville, Curt Struck, Naoshi Sugiyama, Rashid Sunyaev, and Scott Tremaine for stimulating discussions, and the referee for helpful comments. YL gratefully acknowledges an Institute for Theory and Computation Fellowship, and financial support from the Grants-in-Aid for Young Scientists A17684008 by MEXT (Japan) for a visit to Nagoya. BR was supported in part by NASA through the Spitzer Space Telescope Fellowship Program through a contract issued by the Jet Propulsion Laboratory, California Institute of Technology, under a contract with NASA. NY acknowledges support from the Grants-in-Aid for Young Scientists A17684008 by MEXT. The computations reported here were performed at the Center for Parallel Astrophysical Computing at Harvard-Smithsonian Center for Astrophysics, while the initial conditions for the cosmological simulations were created on the COSMOLOGY MACHINE supercomputer at the Institute for Computational Cosmology in Durham. This work was supported in part by NSF grant 03-07690 and NASA ATP grant NAG5-13381.

## REFERENCES

- Abel, T., Bryan, G. L., & Norman, M. L. 2002, *Science*, 295, 93
- Abel, T., Wise, J. H., & Bryan, G. L. 2006, ArXiv Astrophysics e-prints
- Ajiki, M., Taniguchi, Y., Murayama, T., Nagao, T., Veilleux, S., Shioya, Y., Fujita, S. S., Kakazu, Y., Komiyama, Y., Okamura, S., Sanders, D. B., Oyabu, S., Kawara, K., Ohya, Y., Iye, M., Kashikawa, N., Yoshida, M., Sasaki, T., Kosugi, G., Aoki, K., Takata, T., Saito, Y., Kawabata, K. S., Sekiguchi, K., Okita, K., Shimizu, Y., Inata, M., Ebizuka, N., Ozawa, T., Yadoumaru, Y., Taguchi, H., Ando, H., Nishimura, T., Hayashi, M., Ogasawara, R., & Ichikawa, S.-i. 2002, *ApJ*, 576, L25
- Alexander, D. M., Smail, I., Bauer, F. E., Chapman, S. C., Blain, A. W., Brandt, W. N., & Ivison, R. J. 2005, *Nature*, 434, 738
- Bahcall, J. N., Kirhakos, S., Saxe, D. H., & Schneider, D. P. 1997, *ApJ*, 479, 642
- Baker, J. G., Centrella, J., Choi, D.-I., Koppitz, M., van Meter, J. R., & Miller, M. C. 2006, *ApJ*, 653, L93
- Barkana, R., & Loeb, A. 2001, *Phys. Rep.*, 349, 125
- Barnes, J., & Hut, P. 1986, *Nature*, 324, 446
- Barnes, J. E. 2002, *MNRAS*, 333, 481
- Barnes, J. E., & Hernquist, L. 1992, *ARA&A*, 30, 705
- , 1996, *ApJ*, 471, 115
- Barnes, J. E., & Hernquist, L. E. 1991, *ApJ*, 370, L65
- Barth, A. J., Martini, P., Nelson, C. H., & Ho, L. C. 2003, *ApJ*, 594, L95
- Barton, E. J., Davé, R., Smith, J.-D. T., Papovich, C., Hernquist, L., & Springel, V. 2004, *ApJ*, 604, L1
- Becker, G. D., Sargent, W. L. W., Rauch, M., & Simcoe, R. A. 2006, *ApJ*, 640, 69
- Becker, R. H., Fan, X., White, R. L., Strauss, M. A., Narayanan, V. K., Lupton, R. H., Gunn, J. E., Annis, J., Bahcall, N. A., Brinkmann, J., Connolly, A. J., Csabai, I., Czarapata, P. C., Doi, M., Heckman, T. M., Hennessy, G. S., Ivezić, Ž., Knapp, G. R., Lamb, D. Q., McKay, T. A., Munn, J. A., Nash, T., Nichol, R., Pier, J. R., Richards, G. T., Schneider, D. P., Stoughton, C., Szalay, A. S., Thakar, A. R., & York, D. G. 2001, *AJ*, 122, 2850
- Beelen, A., Cox, P., Benford, D. J., Dowell, C. D., Kovács, A., Bertoldi, F., Omont, A., & Carilli, C. L. 2006, *ApJ*, 642, 694
- Begelman, M. C., Blandford, R. D., & Rees, M. J. 1980, *Nature*, 287, 307
- Begelman, M. C., Volonteri, M., & Rees, M. J. 2006, *MNRAS*, 370, 289
- Bertoldi, F., Carilli, C. L., Cox, P., Fan, X., Strauss, M. A., Beelen, A., Omont, A., & Zylka, R. 2003a, *A&A*, 406, L55
- Bertoldi, F., Cox, P., Neri, R., Carilli, C. L., Walter, F., Omont, A., Beelen, A., Henkel, C., Fan, X., Strauss, M. A., & Menten, K. M. 2003b, *A&A*, 409, L47
- Binney, J., & Tremaine, S. 1987, *Galactic dynamics* (Princeton, NJ, Princeton University Press, 1987, 747 p.)
- Blanchet, L., Qusailah, M. S. S., & Will, C. M. 2005, *ApJ*, 635, 508
- Bogdanovic, T., Reynolds, C. S., & Miller, M. C. 2007, *astro-ph/0703054*
- Bondi, H. 1952, *MNRAS*, 112, 195
- Bondi, H., & Hoyle, F. 1944, *MNRAS*, 104, 273
- Bonnor, W. B., & Rotenberg, M. A. 1961, *Royal Society of London Proceedings Series A*, 265, 109
- Borys, C., Smail, I., Chapman, S. C., Blain, A. W., Alexander, D. M., & Ivison, R. J. 2005, *ApJ*, 635, 853
- Bouwens, R. J., Illingworth, G. D., Thompson, R. I., Blakeslee, J. P., Dickinson, M. E., Broadhurst, T. J., Eisenstein, D. J., Fan, X., Franx, M., Meurer, G., & van Dokkum, P. 2004, *ApJ*, 606, L25
- Bouwens, R. J., Illingworth, G. D., Thompson, R. I., & Franx, M. 2005, *ApJ*, 624, L5
- Brinchmann, J., Charlot, S., White, S. D. M., Tremonti, C., Kauffmann, G., Heckman, T., & Brinkmann, J. 2004, *MNRAS*, 351, 1151
- Bromm, V., & Larson, R. B. 2004, *ARA&A*, 42, 79
- Bromm, V., & Loeb, A. 2003, *ApJ*, 596, 34
- Bruzual, G., & Charlot, S. 2003, *MNRAS*, 344, 1000
- Bullock, J. S., Kolatt, T. S., Sigad, Y., Somerville, R. S., Kravtsov, A. V., Klypin, A. A., Primack, J. R., & Dekel, A. 2001, *MNRAS*, 321, 559
- Bunker, A. J., Stanway, E. R., Ellis, R. S., & McMahon, R. G. 2004, *MNRAS*, 355, 374
- Campanelli, M., Lousto, C. O., Zlochower, Y., & Merritt, D. 2007, *ApJ*, in press, *gr-qc/0701164*
- Carilli, C. L., Walter, F., Bertoldi, F., Menten, K. M., Fan, X., Lewis, G. F., Strauss, M. A., Cox, P., Beelen, A., Omont, A., & Mohan, N. 2004, *AJ*, 128, 997
- Carr, B. J., Bond, J. R., & Arnett, W. D. 1984, *ApJ*, 277, 445
- Chakrabarti, S., Cox, T. J., Hernquist, L., Hopkins, P. F., Robertson, B., & Di Matteo, T. 2006, *astro-ph/0605652*
- Chakrabarti, S., Uchida, K. I., Weedman, D., Herter, T., Houck, J. R., Teplitz, H. I., Armus, L., Brandl, B. R., Higdon, S. J. U., Soifer, B. T., Appleton, P. N., van Cleve, J., & Higdon, J. L. 2004, *ApJS*, 154, 142
- Conselice, C. J., Bershad, M. A., Dickinson, M., & Papovich, C. 2003, *AJ*, 126, 1183
- Cox, T. J., Chakrabarti, S., Di Matteo, T., Hernquist, L., Hopkins, P. F., Krause, E., Li, Y., Robertson, B., & Springel, V. 2006a, in preparation
- Cox, T. J., Di Matteo, T., Hernquist, L., Hopkins, P. F., Robertson, B., & Springel, V. 2006b, *ApJ*, 643, 692
- Cox, T. J., Dutta, S. N., Di Matteo, T., Hernquist, L., Hopkins, P. F., Robertson, B., & Springel, V. 2006c, *ApJ*, in press, *astro-ph/0607446*
- Damour, T., & Gopakumar, A. 2006, *Phys. Rev. D*, 73, 124006
- Dasyra, K. M., Tacconi, L. J., Davies, R. I., Genzel, R., Lutz, D., Naab, T., Burkert, A., Veilleux, S., & Sanders, D. B. 2006, *ApJ*, 638, 745
- Davé, R., Finlator, K., & Oppenheimer, B. D. 2006, *MNRAS*, 370, 273
- Davé, R., Hernquist, L., Katz, N., & Weinberg, D. H. 1999, *ApJ*, 511, 521
- Davis, M., Efstathiou, G., Frenk, C. S., & White, S. D. M. 1985, *ApJ*, 292, 371
- Di Matteo, T., Springel, V., & Hernquist, L. 2005, *Nature*, 433, 604
- Dickinson, M., Stern, D., Giavalisco, M., Ferguson, H. C., Tsvetanov, Z., Chornock, R., Cristiani, S., Dawson, S., Dey, A., Filippenko, A. V., Moustakas, L. A., Nonino, M., Papovich, C., Ravindranath, S., Riess, A., Rosati, P., Spinrad, H., & Vanzella, E. 2004, *ApJ*, 600, L99
- Djorgovski, S. G., Castro, S., Stern, D., & Mahabal, A. A. 2001, *ApJ*, 560, L5
- Dubinski, J. 1998, *ApJ*, 502, 141
- Dwek, E. e. a. 2006, in preparation
- Efstathiou, G., & Rees, M. J. 1988, *MNRAS*, 230, 5P
- Egami, E., Kneib, J.-P., Rieke, G. H., Ellis, R. S., Richard, J., Rigby, J., Papovich, C., Stark, D., Santos, M. R., Huang, J.-S., Dole, H., Le Floch, E., & Pérez-González, P. G. 2005, *ApJ*, 618, L5
- Elvis, M., Wilkes, B. J., McDowell, J. C., Green, R. F., Bechtold, J., Willner, S. P., Oey, M. S., Polonski, E., & Cutri, R. 1994, *ApJS*, 95, 1
- Escala, A., Larson, R. B., Coppi, P. S., & Mardones, D. 2004, *ApJ*, 607, 765
- Eyles, L., Bunker, A., Ellis, R., Lacy, M., Stanway, E., Stark, D., & Chiu, K. 2006, *astro-ph/0607306*
- Eyles, L. P., Bunker, A. J., Stanway, E. R., Lacy, M., Ellis, R. S., & Doherty, M. 2005, *MNRAS*, 364, 443
- Fabian, A. C. 1999, *MNRAS*, 308, L39
- Fan, X. 2006, *Memorie della Societa Astronomica Italiana*, 77, 635
- Fan, X., Carilli, C. L., & Keating, B. 2006, *ARA&A*, 44, 415
- Fan, X., Hennawi, J. F., Richards, G. T., Strauss, M. A., Schneider, D. P., Donley, J. L., Young, J. E., Annis, J., Lin, H., Lampeitl, H., Lupton, R. H., Gunn, J. E., Knapp, G. R., Brandt, W. N., Anderson, S., Bahcall, N. A., Brinkmann, J., Brunner, R. J., Fukugita, M., Szalay, A. S., Szokoly, G. P., & York, D. G. 2004, *AJ*, 128, 515
- Fan, X., Narayanan, V. K., Lupton, R. H., Strauss, M. A., Knapp, G. R., Becker, R. H., White, R. L., Pentericci, L., Leggett, S. K., Haiman, Z., Gunn, J. E., Ivezić, Ž., Schneider, D. P., Anderson, S. F., Brinkmann, J., Bahcall, N. A., Connolly, A. J., Csabai, I., Doi, M., Fukugita, M., Geballe, T., Grebel, E. K., Harbeck, D., Hennessy, G., Lamb, D. Q., Miknaitis, G., Munn, J. A., Nichol, R., Okamura, S., Pier, J. R., Prada, F., Richards, G. T., Szalay, A., & York, D. G. 2001, *AJ*, 122, 2833
- Fan, X., Strauss, M. A., Schneider, D. P., Becker, R. H., White, R. L., Haiman, Z., Gregg, M., Pentericci, L., Grebel, E. K., Narayanan, V. K., Loh, Y.-S., Richards, G. T., Gunn, J. E., Lupton, R. H., Knapp, G. R., Ivezić, Ž., Brandt, W. N., Collinge, M., Hao, L., Harbeck, D., Prada, F., Schaye, J., Strateva, I., Zakamska, N., Anderson, S., Brinkmann, J., Bahcall, N. A., Lamb, D. Q., Okamura, S., Szalay, A., & York, D. G. 2003, *AJ*, 125, 1649
- Favata, M., Hughes, S. A., & Holz, D. E. 2004, *ApJ*, 607, L5
- Ferrarese, L., & Merritt, D. 2000, *ApJ*, 539, L9
- Fitchett, M. J. 1983, *MNRAS*, 203, 1049
- Flanagan, É. É., & Hughes, S. A. 1998, *Phys. Rev. D*, 57, 4535
- Folkner, W. M. 1998, in AIP Conf. Proc. 456: *Laser Interferometer Space Antenna*, Second International LISA Symposium on the Detection and Observation of Gravitational Waves in Space, ed. W. M. Folkner, 11–16
- Fryer, C. L., Woosley, S. E., & Heger, A. 2001, *ApJ*, 550, 372
- Gao, L., Abel, T., Frenk, C. S., Jenkins, A., Springel, V., & Yoshida, N. 2006, *astro-ph/0610174*
- Gao, L., White, S. D. M., Jenkins, A., Frenk, C. S., & Springel, V. 2005, *MNRAS*, 363, 379

- Gebhardt, K., Bender, R., Bower, G., Dressler, A., Faber, S. M., Filippenko, A. V., Green, R., Grillmair, C., Ho, L. C., Kormendy, J., Lauer, T. R., Magorrian, J., Pinkney, J., Richstone, D., & Tremaine, S. 2000, *ApJ*, 539, L13
- Giavalisco, M., Dickinson, M., Ferguson, H. C., Ravindranath, S., Kretchmer, C., Moustakas, L. A., Madau, P., Fall, S. M., Gardner, J. P., Livio, M., Papovich, C., Renzini, A., Spinrad, H., Stern, D., & Riess, A. 2004, *ApJ*, 600, L103
- Glikman, E., Helfand, D. J., & White, R. L. 2006, *ApJ*, 640, 579
- Gonzalez, J. A., Hannam, M. D., Sperhake, U., Bruggmann, B., & Husa, S. 2007, *gr-qc/0702052*
- Gonzalez, J. A., Sperhake, U., Bruegmann, B., Hannam, M., & Husa, S. 2006, *Physical Review Letters*, in press, *gr-qc/0610154*
- Graham, A. W., Erwin, P., Caon, N., & Trujillo, I. 2001, *ApJ*, 563, L11
- Greene, J. E., & Ho, L. C. 2006, *ApJ*, 641, L21
- Gunn, J. E., & Peterson, B. A. 1965, *ApJ*, 142, 1633
- Haehnelt, M. G. 1998, in *AIP Conf. Proc. 456: Laser Interferometer Space Antenna, Second International LISA Symposium on the Detection and Observation of Gravitational Waves in Space*, ed. W. M. Folkner, 45–49
- Haehnelt, M. G., Natarajan, P., & Rees, M. J. 1998, *MNRAS*, 300, 817
- Haiman, Z. 2004, *ApJ*, 613, 36
- . 2006, *New Astronomy Review*, 50, 672
- Haiman, Z., & Loeb, A. 2001, *ApJ*, 552, 459
- Heckman, T. M., Bothun, G. D., Balick, B., & Smith, E. P. 1984, *AJ*, 89, 958
- Heckman, T. M., Lehnert, M. D., Strickland, D. K., & Armus, L. 2000, *ApJS*, 129, 493
- Heger, A., Fryer, C. L., Woosley, S. E., Langer, N., & Hartmann, D. H. 2003, *ApJ*, 591, 288
- Hernquist, L. 1989, *Nature*, 340, 687
- . 1990, *ApJ*, 356, 359
- . 1993, *ApJS*, 86, 389
- Hernquist, L., & Katz, N. 1989, *ApJS*, 70, 419
- Hernquist, L., & Mihos, J. C. 1995, *ApJ*, 448, 41
- Hernquist, L., & Springel, V. 2003, *MNRAS*, 341, 1253
- Herrmann, F., Hinder, I., Shoemaker, D., Laguna, P., & Matzner, R. A. 2007, *ApJ*, in press, *gr-qc/0701143*
- Herrmann, F., Shoemaker, D., & Laguna, P. 2006, *ArXiv General Relativity and Quantum Cosmology e-prints*
- Hines, D. C., Krause, O., Rieke, G. H., Fan, X., Blaylock, M., & Neugebauer, G. 2006, *ApJ*, 641, L85
- Hockney, R. W., & Eastwood, J. W. 1981, *Computer Simulation Using Particles* (Computer Simulation Using Particles, New York: McGraw-Hill, 1981)
- Hopkins, P. F., & Hernquist, L. 2006, *ApJS*, in press, *astro-ph/0603180*
- Hopkins, P. F., Hernquist, L., Cox, T. J., Di Matteo, T., Martini, P., Robertson, B., & Springel, V. 2005a, *ApJ*, 630, 705
- Hopkins, P. F., Hernquist, L., Cox, T. J., Di Matteo, T., Robertson, B., & Springel, V. 2005b, *ApJ*, 630, 716
- . 2005c, *ApJ*, 632, 81
- . 2006a, *ApJS*, 163, 1
- Hopkins, P. F., Hernquist, L., Cox, T. J., Robertson, B., Di Matteo, T., & Springel, V. 2006b, *ApJ*, 639, 700
- Hopkins, P. F., Hernquist, L., Cox, T. J., Robertson, B., & Krause, E. 2007, *ArXiv Astrophysics e-prints*
- Hopkins, P. F., Hernquist, L., Cox, T. J., Robertson, B., & Springel, V. 2006c, *ApJS*, 163, 50
- Hopkins, P. F., Hernquist, L., Martini, P., Cox, T. J., Robertson, B., Di Matteo, T., & Springel, V. 2005d, *ApJ*, 625, L71
- Hopkins, P. F., Richards, G. T., & Hernquist, L. 2006d, *ApJ*, submitted, *astro-ph/0605678*
- Hopkins, P. F., Somerville, R. S., Hernquist, L., Cox, T. J., Robertson, B., & Li, Y. 2006e, *ApJ*, submitted, *astro-ph/0602290*
- Horton, A., Parry, I., Bland-Hawthorn, J., Cianci, S., King, D., McMahon, R., & Medlen, S. 2004, in *Ground-based Instrumentation for Astronomy*. Edited by Alan F. M. Moorwood and Iye Masanori. *Proceedings of the SPIE*, Volume 5492, pp. 1022-1032 (2004), ed. A. F. M. Moorwood & M. Iye, 1022–1032
- Hoyle, F., & Lyttleton, R. A. 1941, *MNRAS*, 101, 227
- Hu, E. M., & Cowie, L. L. 2006, *Nature*, 440, 1145
- Hu, E. M., Cowie, L. L., McMahon, R. G., Capak, P., Iwamuro, F., Kneib, J.-P., Maihara, T., & Motohara, K. 2002, *ApJ*, 568, L75
- Hughes, S. A. 2002, *MNRAS*, 331, 805
- Hutchings, J. B. 2005, *PASP*, 117, 1250
- Hutchings, J. B., & Neff, S. G. 1992, *AJ*, 104, 1
- Jenkins, A., Frenk, C. S., White, S. D. M., Colberg, J. M., Cole, S., Evrard, A. E., Couchman, H. M. P., & Yoshida, N. 2001, *MNRAS*, 321, 372
- Jiang, L., Fan, X., Hines, D. C., Shi, Y., Vestergaard, M., Bertoldi, F., Brandt, W. N., Carilli, C. L., Cox, P., Le Floc'h, E., Pentericci, L., Richards, G. T., Rieke, G. H., Schneider, D. P., Strauss, M. A., Walter, F., & Brinkmann, J. 2006, *AJ*, in press, *astro-ph/0608006*
- Jogee, S. 2006, in *Physics of Active Galactic Nuclei at all Scales*, ed. D. Alloin, R. Johnson, and P. Lira (Berlin: Springer), 143
- Johnson, J. L., & Bromm, V. 2006, *MNRAS*, in press, *astro-ph/0605691*
- Katz, N., Weinberg, D. H., & Hernquist, L. 1996, *ApJS*, 105, 19
- Kazantzidis, S., Mayer, L., Colpi, M., Madau, P., Debattista, V. P., Wadsley, J., Stadel, J., Quinn, T., & Moore, B. 2005, *ApJ*, 623, L67
- Kennicutt, R. C. 1998, *ApJ*, 498, 541
- Khochfar, S., & Burkert, A. 2006, *A&A*, 445, 403
- King, A. 2003, *ApJ*, 596, L27
- Kollmeier, J. A., Onken, C. A., Kochanek, C. S., Gould, A., Weinberg, D. H., Dietrich, M., Cool, R., Dey, A., Eisenstein, D. J., Jannuzi, B. T., Le Floc'h, E., & Stern, D. 2005, *ApJ*, in press, *astro-ph/0508657*
- Koushiappas, S. M., & Zentner, A. R. 2006, *ApJ*, 639, 7
- Lacey, C., & Cole, S. 1993, *MNRAS*, 262, 627
- Li, Y. 2007, in preparation
- Li, Y., Haiman, Z., & Mac Low, M.-M. 2006a, *ApJ*, submitted, *astro-ph/0607444*
- Li, Y., Hernquist, L., Finkbeiner, D., Fan, X., & Jiang, L. 2007, in preparation
- Li, Y., Mac Low, M.-M., & Klessen, R. S. 2004, *ApJ*, 614, L29
- . 2005, *ApJ*, 620, L19
- . 2006b, *ApJ*, 639, 879
- Lidz, A., Hui, L., Zaldarriaga, M., & Scoccimarro, R. 2002, *ApJ*, 579, 491
- Loeb, A., & Barkana, R. 2001, *ARA&A*, 39, 19
- Loeb, A., & Rasio, F. A. 1994, *ApJ*, 432, 52
- Lynden-Bell, D. 1969, *Nature*, 223, 690
- Madau, P., Ferguson, H. C., Dickinson, M. E., Giavalisco, M., Steidel, C. C., & Fruchter, A. 1996, *MNRAS*, 283, 1388
- Madau, P., & Quataert, E. 2004, *ApJ*, 606, L17
- Magorrian, J., Tremaine, S., Richstone, D., Bender, R., Bower, G., Dressler, A., Faber, S. M., Gebhardt, K., Green, R., Grillmair, C., Kormendy, J., & Lauer, T. 1998, *AJ*, 115, 2285
- Maiolino, R., Cox, P., Caselli, P., Beelen, A., Bertoldi, F., Carilli, C. L., Kaufman, M. J., Menten, K. M., Nagao, T., Omont, A., Weiß, A., Walmsley, C. M., & Walter, F. 2005, *A&A*, 440, L51
- Malhotra, S., & Rhoads, J. E. 2004, *ApJ*, 617, L5
- Marconi, A., & Hunt, L. K. 2003, *ApJ*, 589, L21
- Marconi, A., Risaliti, G., Gilli, R., Hunt, L. K., Maiolino, R., & Salvati, M. 2004, *MNRAS*, 351, 169
- Martin, C. L. 1999, *ApJ*, 513, 156
- . 2005, *ApJ*, 621, 227
- Menou, K., Haiman, Z., & Narayanan, V. K. 2001, *ApJ*, 558, 535
- Merritt, D., Milosavljević, M., Favata, M., Hughes, S. A., & Holz, D. E. 2004, *ApJ*, 607, L9
- Meurer, G. R., Heckman, T. M., Lehnert, M. D., Leitherer, C., & Lowenthal, J. 1997, *AJ*, 114, 54
- Mihos, J. C., & Hernquist, L. 1994, *ApJ*, 425, L13
- . 1996, *ApJ*, 464, 641
- Milosavljević, M., & Merritt, D. 2003, *ApJ*, 596, 860
- Mo, H. J., Mao, S., & White, S. D. M. 1998, *MNRAS*, 295, 319
- Mobasher, B., Dickinson, M., Ferguson, H. C., Giavalisco, M., Wiklind, T., Stark, D., Ellis, R. S., Fall, S. M., Grogin, N. A., Moustakas, L. A., Panagia, N., Sosey, M., Stiavelli, M., Bergeron, E., Casertano, S., Ingraham, P., Koekemoer, A., Labbé, I., Livio, M., Rodgers, B., Scarlata, C., Vernet, J., Renzini, A., Rosati, P., Kuntschner, H., Kümmel, M., Walsh, J. R., Chary, R., Eisenhardt, P., Pirzkal, N., & Stern, D. 2005, *ApJ*, 635, 832
- Murray, N., Quataert, E., & Thompson, T. A. 2005, *ApJ*, 618, 569
- Naab, T., & Burkert, A. 2003, *ApJ*, 597, 893
- Narayanan, D., Cox, T. J., Robertson, B., Davé, R., Di Matteo, T., Hernquist, L., Hopkins, P., Kulesa, C., & Walker, C. K. 2006a, *ApJ*, 642, L107
- Narayanan, D., Kulesa, C., Boss, A., & Walker, C. K. 2006b, *ApJ*, 647
- Narayanan, D., Li, Y., Cox, T. J., Hernquist, L., Hopkins, P., Chakrabarti, S., Davé, R., Di Matteo, T., Kulesa, C., Robertson, B., Springel, V., & Walker, C. K. 2006c, *ApJ*, submitted
- Navarro, J. F., Frenk, C. S., & White, S. D. M. 1997, *ApJ*, 490, 493
- Norman, C., & Scoville, N. 1988, *ApJ*, 332, 124
- Page, L., Hinshaw, G., Komatsu, E., Nolta, M. R., Spergel, D. N., Bennett, C. L., Barnes, C., Bean, R., Dore, O., Halpern, M., Hill, R. S., Jarosik, N., Kogut, A., Limon, M., Meyer, S. S., Odegard, N., Peiris, H. V., Tucker, G. S., Verde, L., Weiland, J. L., Wollack, E., & Wright, E. L. 2006, *astro-ph/0603450*



- Peng, C. Y., Impey, C. D., Ho, L. C., Barton, E. J., & Rix, H.-W. 2006, *ApJ*, 640, 114
- Peres, A. 1962, *Physical Review*, 128, 2471
- Pettini, M., Rix, S. A., Steidel, C. C., Adelberger, K. L., Hunt, M. P., & Shapley, A. E. 2002, *ApJ*, 569, 742
- Power, C., Navarro, J. F., Jenkins, A., Frenk, C. S., White, S. D. M., Springel, V., Stadel, J., & Quinn, T. 2003, *MNRAS*, 338, 14
- Press, W. H., & Schechter, P. 1974, *ApJ*, 187, 425
- Richards, G. T., Lacy, M., Storrie-Lombardi, L. J., Hall, P. B., Gallagher, S. C., Hines, D. C., Fan, X., Papovich, C., Vanden Berk, D. E., Trammell, G. B., Schneider, D. P., Vestergaard, M., York, D. G., Jester, S., Anderson, S. F., Budavari, T., & Szalay, A. S. 2006, *astro-ph/0601558*
- Robertson, B., Cox, T. J., Hernquist, L., Franx, M., Hopkins, P. F., Martini, P., & Springel, V. 2006a, *ApJ*, 641, 21
- Robertson, B., Hernquist, L., Cox, T. J., Di Matteo, T., Hopkins, P. F., Martini, P., & Springel, V. 2006b, *ApJ*, 641, 90
- Robertson, B., Yoshida, N., Springel, V., & Hernquist, L. 2004, *ApJ*, 606, 32
- Robson, I., Priddey, R. S., Isaak, K. G., & McMahon, R. G. 2004, *MNRAS*, 351, L29
- Rupke, D. S., Veilleux, S., & Sanders, D. B. 2002, *ApJ*, 570, 588
- 2005, *ApJ*, 632, 751
- Salpeter, E. E. 1964, *ApJ*, 140, 796
- Sanders, D. B., & Mirabel, I. F. 1996, *ARA&A*, 34, 749
- Sanders, D. B., Soifer, B. T., Elias, J. H., Madore, B. F., Matthews, K., Neugebauer, G., & Scoville, N. Z. 1988, *ApJ*, 325, 74
- Sazonov, S. Y., Ostriker, J. P., Ciotti, L., & Sunyaev, R. A. 2005, *MNRAS*, 358, 168
- Schechter, P. 1976, *ApJ*, 203, 297
- Schmidt, M. 1959, *ApJ*, 129, 243
- Scoville, N. 2003, *Journal of Korean Astronomical Society*, 36, 167
- Scoville, N. Z., Evans, A. S., Thompson, R., Rieke, M., Hines, D. C., Low, F. J., Dinshaw, N., Surace, J. A., & Armus, L. 2000, *AJ*, 119, 991
- Seljak, U., & Zaldarriaga, M. 1996, *ApJ*, 469, 437
- Sesana, A., Haardt, F., Madau, P., & Volonteri, M. 2005, *ApJ*, 623, 23
- Shakura, N. I., & Sunyaev, R. A. 1973, *A&A*, 24, 337
- Shapley, A. E., Steidel, C. C., Pettini, M., & Adelberger, K. L. 2003, *ApJ*, 588, 65
- Shaver, P. A., Wall, J. V., Kellermann, K. I., Jackson, C. A., & Hawkins, M. R. S. 1996, *Nature*, 384, 439
- Sheth, R. K., & Tormen, G. 2002, *MNRAS*, 329, 61
- Shields, G. A., Gebhardt, K., Salvander, S., Wills, B. J., Xie, B., Brotherton, M. S., Yuan, J., & Dietrich, M. 2003, *ApJ*, 583, 124
- Shields, G. A., Menezes, K. L., Massart, C. A., & Vanden Bout, P. 2006, *ApJ*, 641, 683
- Silk, J., & Rees, M. J. 1998, *A&A*, 331, L1
- Sokasian, A., Abel, T., Hernquist, L., & Springel, V. 2003, *MNRAS*, 344, 607
- Somerville, R. S., Primack, J. R., & Faber, S. M. 2001, *MNRAS*, 320, 504
- Songaila, A., & Cowie, L. L. 2002, *AJ*, 123, 2183
- Spergel, D. N., Bean, R., Dore, O., Nolte, M. R., Bennett, C. L., Hinshaw, G., Jarosik, N., Komatsu, E., Page, L., Peiris, H. V., Verde, L., Barnes, C., Halpern, M., Hill, R. S., Kogut, A., Limon, M., Meyer, S. S., Odegard, N., Tucker, G. S., Weiland, J. L., Wollack, E., & Wright, E. L. 2006, *astro-ph/0603449*
- Spergel, D. N., Verde, L., Peiris, H. V., Komatsu, E., Nolte, M. R., Bennett, C. L., Halpern, M., Hinshaw, G., Jarosik, N., Kogut, A., Limon, M., Meyer, S. S., Page, L., Tucker, G. S., Weiland, J. L., Wollack, E., & Wright, E. L. 2003, *ApJS*, 148, 175
- Springel, V. 2000, *MNRAS*, 312, 859
- 2005, *MNRAS*, 364, 1105
- Springel, V., Di Matteo, T., & Hernquist, L. 2005a, *ApJ*, 620, L79
- 2005b, *MNRAS*, 361, 776
- Springel, V., Frenk, C. S., & White, S. D. M. 2006, *Nature*, 440, 1137
- Springel, V., & Hernquist, L. 2002, *MNRAS*, 333, 649
- 2003a, *MNRAS*, 339, 289
- 2003b, *MNRAS*, 339, 312
- 2005, *ApJ*, 622, L9
- Springel, V., & White, S. D. M. 1999, *MNRAS*, 307, 162
- Springel, V., White, S. D. M., Jenkins, A., Frenk, C. S., Yoshida, N., Gao, L., Navarro, J., Thacker, R., Croton, D., Helly, J., Peacock, J. A., Cole, S., Thomas, P., Couchman, H., Evrard, A., Colberg, J., & Pearce, F. 2005c, *Nature*, 435, 629
- Stern, D., Yost, S. A., Eckart, M. E., Harrison, F. A., Helfand, D. J., Djorgovski, S. G., Malhotra, S., & Rhoads, J. E. 2005, *ApJ*, 619, 12
- Stockton, A. 1978, *ApJ*, 223, 747
- Tan, J. C., & McKee, C. F. 2004, *ApJ*, 603, 383
- Thompson, T. A., Quataert, E., & Murray, N. 2005, *ApJ*, 630, 167
- Thorne, K. S., & Braginskii, V. B. 1976, *ApJ*, 204, L1
- Tremaine, S., Gebhardt, K., Bender, R., Bower, G., Dressler, A., Faber, S. M., Filippenko, A. V., Green, R., Grillmair, C., Ho, L. C., Kormendy, J., Lauer, T. R., Magorrian, J., Pinkney, J., & Richstone, D. 2002, *ApJ*, 574, 740
- Treu, T., Malkan, M. A., & Blandford, R. D. 2004, *ApJ*, 615, L97
- Veilleux, S., Cecil, G., & Bland-Hawthorn, J. 2005, *ARA&A*, 43, 769
- Veilleux, S., Kim, D.-C., & Sanders, D. B. 2002, *ApJS*, 143, 315
- Vestergaard, M. 2004, *ApJ*, 601, 676
- Vestergaard, M., & Fan, X. 2006, in preparation
- Vestergaard, M., & Peterson, B. M. 2006, *ApJ*, 641, 689
- Volonteri, M., & Rees, M. J. 2005, *ApJ*, 633, 624
- 2006, *ApJ*, 650, 669
- Walter, F., Bertoldi, F., Carilli, C., Cox, P., Lo, K. Y., Neri, R., Fan, X., Omont, A., Strauss, M. A., & Menten, K. M. 2003, *Nature*, 424, 406
- Walter, F., Carilli, C., Bertoldi, F., Menten, K., Cox, P., Lo, K. Y., Fan, X., & Strauss, M. A. 2004, *ApJ*, 615, L17
- White, R. L., Becker, R. H., Fan, X., & Strauss, M. A. 2003, *AJ*, 126, 1
- 2005, *AJ*, 129, 2102
- Willott, C. J., McLure, R. J., & Jarvis, M. J. 2003, *ApJ*, 587, L15
- Willott, C. J., Percival, W. J., McLure, R. J., Crampton, D., Hutchings, J. B., Jarvis, M. J., Sawicki, M., & Simard, L. 2005, *ApJ*, 626, 657
- Windhorst, R. A., Cohen, S. H., Jansen, R. A., Conselice, C., & Yan, H. 2006, *New Astronomy Review*, 50, 113
- Wu, X.-B. 2006, *ApJ*, in press, 11415
- Wyithe, J. S. B., & Loeb, A. 2003, *ApJ*, 595, 614
- 2005, *ApJ*, 634, 910
- Xu, G. 1995, *ApJS*, 98, 355
- Yan, H., Dickinson, M., Giavalisco, M., Stern, D., Eisenhardt, P. R. M., & Ferguson, H. C. 2006, *astro-ph/0604554*
- Yan, H., Dickinson, M., Stern, D., Eisenhardt, P. R. M., Chary, R.-R., Giavalisco, M., Ferguson, H. C., Casertano, S., Conselice, C. J., Papovich, C., Reach, W. T., Grogan, N., Moustakas, L. A., & Ouchi, M. 2005, *ApJ*, 634, 109
- Yoo, J., & Miralda-Escudé, J. 2004, *ApJ*, 614, L25
- York, D. G., Adelman, J., & Anderson, Jr., J. E. e. a. 2000, *AJ*, 120, 1579
- Yoshida, N., Oh, S. P., Kitayama, T., & Hernquist, L. 2007, *ApJ*, submitted, *astro-ph/0610819*
- Yoshida, N., Omukai, K., Hernquist, L., & Abel, T. 2006, *ApJ*, 652, 6